Supporting Information

Multi-Arm Junctions for Dynamic DNA Nanotechnology

Shohei Kotani & William L. Hughes*

Micron School of Materials Science & Engineering, Boise State University,
1910 University Dr., Boise, ID, 83725, USA.

Contents:

S1. Proposed reaction mechanism of a three-arm junction substrate

The overall reaction converts two molecules of substrates S1 and S2 into three molecules of products P1, P2, and P3 (Figure S1A), which provides an entropy gain[1] as the driving force. In addition, imperfect base parings at the three-arm junction point[2] of S1 and S2 disappear by the reaction, which also provides base paring gains. For the construction of signal cascades, the single-stranded tails on each substrate (domains α and β of S1, domains γ and δ of S2) can be used to generate outputs with new combinations of domains (domains α and δ of P1, domains γ and β of P2) by the associative toehold mechanism.[3]

The key concept of the system is the large difference of the energy barrier between the catalytic and leakage pathways. In the catalytic pathway (Figure S1B), S1 first consumes the catalyst C1 to produce P1 and the intermediate I1 (step **I**). Then, I1 reacts with S2 to produce C1 and the intermediate I2 (step **II**). Those reactions proceeds through three-way branch migration, and the Intuitive Energy Landscape (IEL) of those reactions show the absence of significant energy barriers after the initiation of the strand displacement, which will allow quick reactions. Finally, I2 is converted into P2 and P3 through four-way branch migration (step **III**) without a reverse reaction, because the long hybridized region (domains c-a-2) in I2 secures the success of the reaction.

In contrast with the catalytic reaction, the leakage reaction is designed to have a high energy barrier. As an example, when a leakage occurs (Figure S1C), the initial step is the hybridization of the domain 1* of S1 and 1 of S2 (The left most state to the second state). This reaction occurs via a zero toehold through three-way branch migration.[4] After the hybridization at domain 1, the system needs to overcome an additional energy barrier to shift into four-way branch migration (the second state to the third state) because of the higher sawtooth amplitude of four-way branch migration. This energy barrier, which is shown as $\Delta E1$, is expected to strongly bias the branch migration backward and slow down the reaction speed by orders of magnitude.

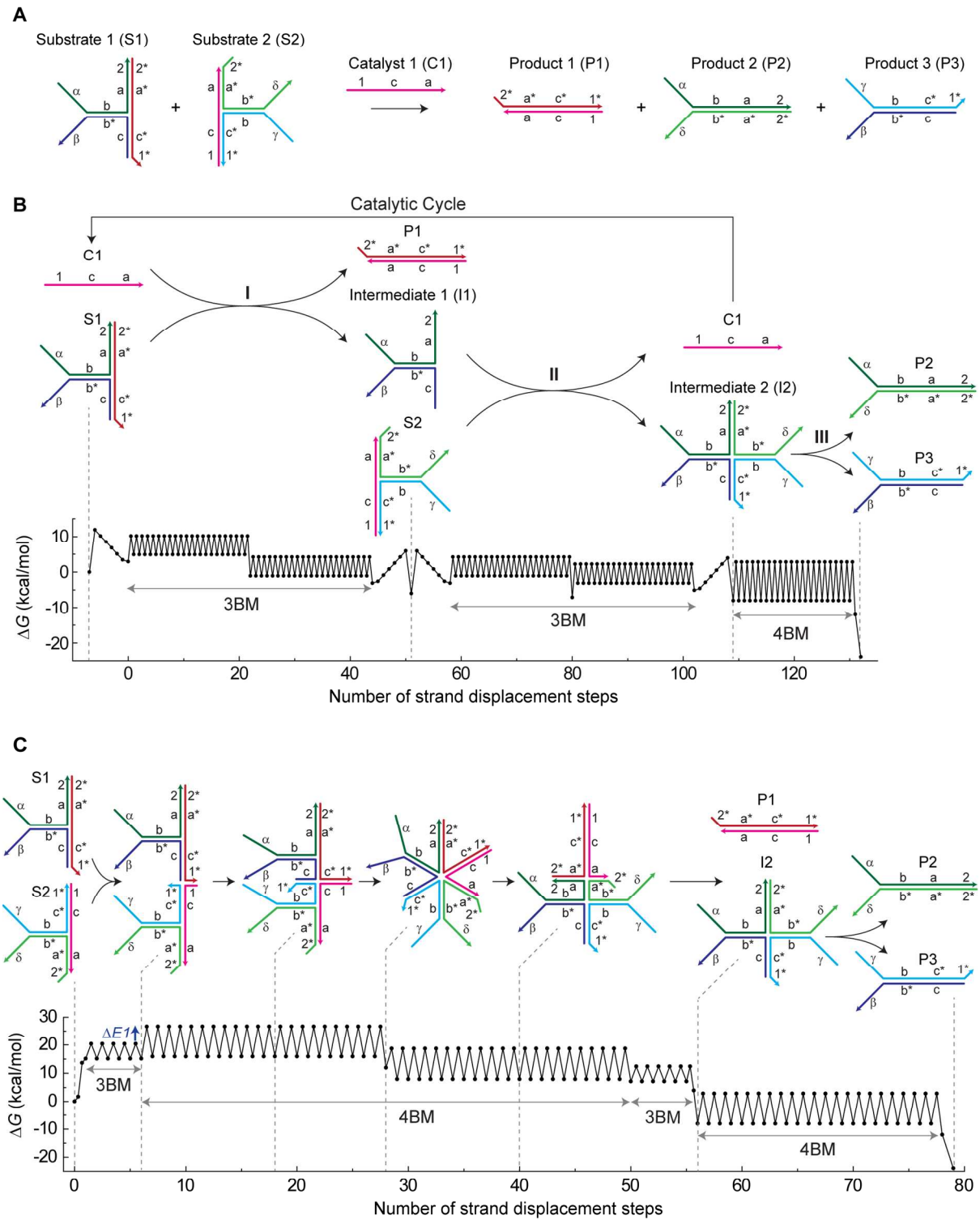

Figure S1. Design principles of a three-arm junction substrate for a catalytic system. (A) A general design and its overall reaction of three-arm junction substrates. Functionalities of DNA sequences are

represented by domains, which are unique segments of continuous oligonucleotides. Asterisk represents complementary domains. Toehold domains are represented by numbers, specificity domains are letters, and output domains are Greek letters. The reaction converts two substrates S1 and S2 into three products P1, P2, and P3. Products P2 and P3 have the new combination of output domains α and δ, γ and β, respectively. The sequences of those outputs are independent of the catalyst C1 (domains 1-c-a), therefore can be used for signal cascades. **(B)** The proposed catalytic reaction pathway. 3BM stands for three-way branch migration, and 4BM stands for four-way branch migration. Step **I** is the reaction between C1 and S1 through three-way branch migration to produce P1 and the intermediate I1. Step **II** is the reaction between I1 and S2 through three-way branch migration to produce C1 and the intermediate I2. Step **III** is the production of P2 and P3 from I2 through four-way branch migration. Also shown is the corresponding Intuitive Energy Landscape (IEL) of each reaction. The details of the IELs are shown in Figure S2A-C. **(C)** The proposed leakage pathway in the absence of a catalyst. While leakage starting from the hybridization of domain 1 is shown, two other leakage pathways (starting from domain 2 or b) are possible and not shown. Because of the existence of the energy barrier Δ*E1* at the transition from three-way branch migration to four-way branch migration, shown in the IEL, the branch migration will be strongly biased backward. The details of the IEL are shown in Figure S2D.

S2. The Intuitive Energy Landscape (IEL) of elementary reactions for three-arm junction substrates

The values of those energy parameters (Δ*Ginit*, Δ*Gbp*, Δ*G1ov*, Δ*G2ov*, Δ*Gp*, Δ*Gs3*) were from a study on three-way branch migration.[5] Briefly, Δ*Ginit* = 11.9 kcal/mol is the free energy cost to localize two separate molecules together with correct orientation. -Δ*Gbp* = -1.7 kcal/mol is the average value of free energy gain to form a base pair. Δ*G1ov* = 1.2 kcal/mol is the free energy cost of introducing a single-stranded DNA overhang at an overhang-free nick. Δ*G2ov* = 3.2 kcal/mol is the free energy cost of introducing two single-stranded DNA overhangs at an overhang-free nick. Δ*Gp* = 2 kcal/mol, "plateau height", is the free energy cost of adding a second tail at a junction already possessing one single-stranded DNA tail (thus, Δ*Gp* = Δ*G2ov* - Δ*G1ov*). Δ*Gs3* = 5.3 kcal/mol "sawtooth amplitude", is the free energy cost for each step of three-way branch migration due to its structural rearrangement.

The values for the structural energy parameters (*ΔG3ajt*, *ΔG3aj*) were calculated as following. *ΔG3ajt* = 5 kcal/mol is the free energy cost of three-arm junction with 2nt thymidine (T2) bulge, assumed the value to be the same as a three-arm junction with 2nt adenine bulge.[6] Δ*G3aj* = 6 kcal/mol is the free energy cost of a three-arm junction without a bulge, deduced from the stabilization effect (-1 kcal/mol) of T2 bulge.[7]

The value of the Δ*Gs4,* sawtooth amplitude of four-way branch migration, was calculated as following. The step time is ~100 μs for three-way branch migration[8] and ~1 s for four-way branch migration.[9] Consequently, their energy barrier difference for each migration step, Δ*G*, can be expected so that

$10^4 = e^{\Delta G/RT}$, resulting in ΔG = 5.5 kcal/mol. Therefore, $\Delta Gs4 = \Delta G + \Delta Gs3$ = 10.8 kcal/mol. In the study of toehold-mediated strand displacement through four-way branch migration,[10] it was hypothesized that the energy barrier to initiate four-way branch migration originates from the "entropic cost of forming a loop", whose value is ~11 kcal/mol. Although this value was used to explain their kinetic data well enough, it is not clear how to compare this large free energy cost with the small cost of forming a four-arm junction, ~1 kcal/mol, measured at 18 °C.[11] The similar value of $\Delta Gs4$ indicates that the large sawtooth amplitude can be the alternative way to explain their data.

Although the free energy cost of a four-arm junction was studied,[11] the calculated value at 25 °C that was based on the study turned out to be too small. Therefore, we instead used the $\Delta G4aj$ = 4 kcal/mol,[12] which was calculated using Mfold.[13] The value is in agreement with the study showing more stability of a four-arm junction than a three-arm junction.[14] For a six-arm junction, the predicted free energy cost by Mfold, ~6 kcal/mol, seemed to be too small considering the less stability of a six-arm junction than a three-arm junction.[15] Therefore, $\Delta G6aj$ = 12 kcal/mol was used simply as twice of a three-arm junction to be conservative.

For Figure S2A, D-G, 0 kcal/mol was set to be the initial free energy of the system. For Figure S2B, C, the initial free energy was set to be the final value of the previous steps.

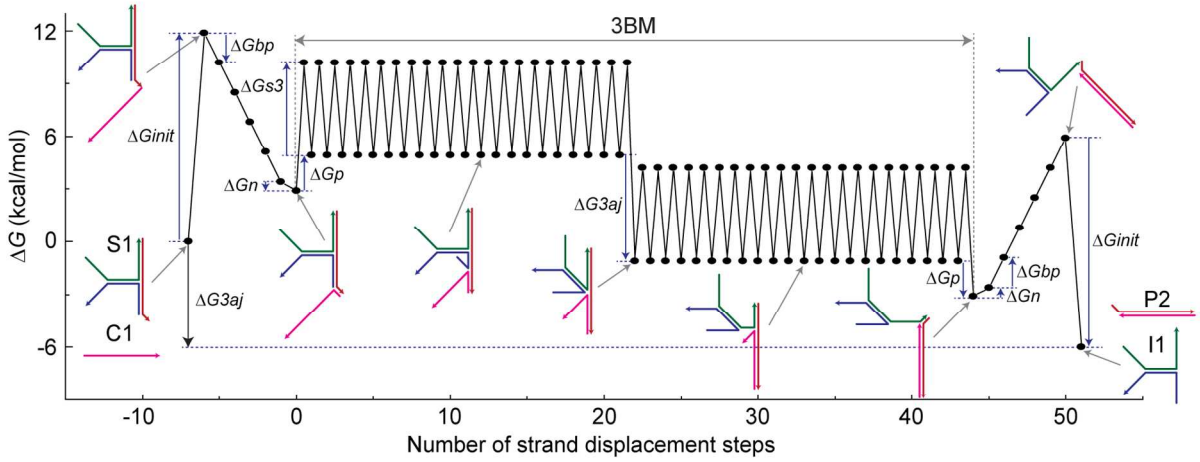

Figure S2A. The detailed IEL for step I. The thermodynamic driving force of the reaction is the elimination of the three-arm junction point in S1. The process of the toehold dissociation at the end of the reaction is shown as sequential dissociations of base pairs in the toehold domain, 1 bp on each step. However, it was shown that the last several base pairs at the end of a strand displacement can dissociate together spontaneously.[16] Although such alternative pathways are not shown here or for other IELs, it is likely that such an alternative pathway is dominant in toehold exchange reactions. Although a few base pairs at the branch-point of a three-arm junction was shown to be unpaired,[2] it was not shown here and our other IELs. 3BM represents three-way branch migration. ΔGn = 0.5 kcal/mol is the sum of a base pair

gain (-Δ*Gbp* = -1.7 kcal/mol) and the cost of introducing a single-stranded DNA overhang at an overhang-free nick (Δ*G1ov* = 1.2 kcal/mol), thus | -Δ*Gbp* + Δ*G1ov* |.

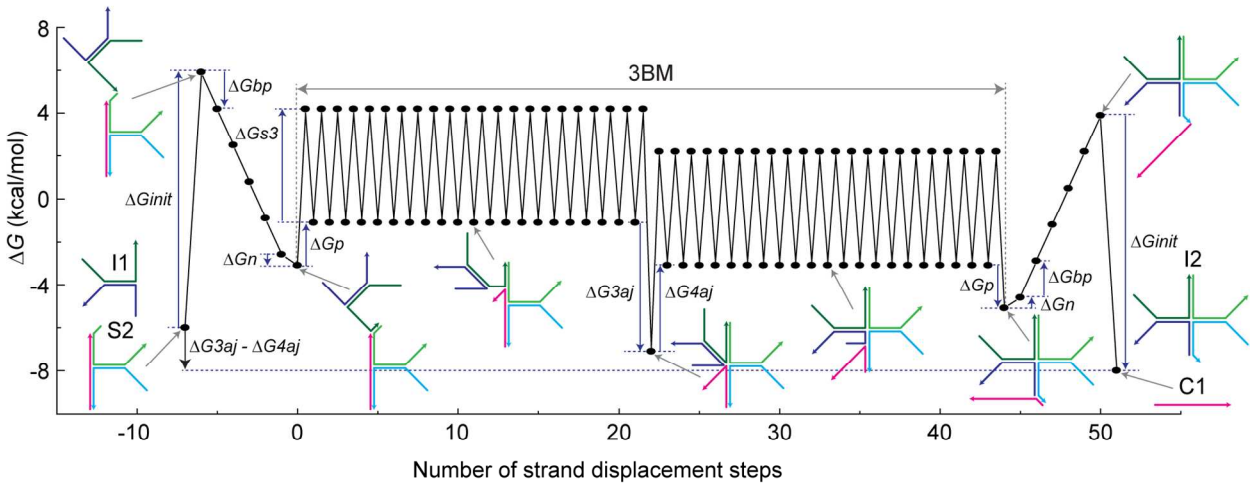

Figure S2B. The detailed IEL for step II. The thermodynamic driving force for the reaction is the elimination at the three-arm junction point in S2 against the formation of the four-arm junction point in I2.

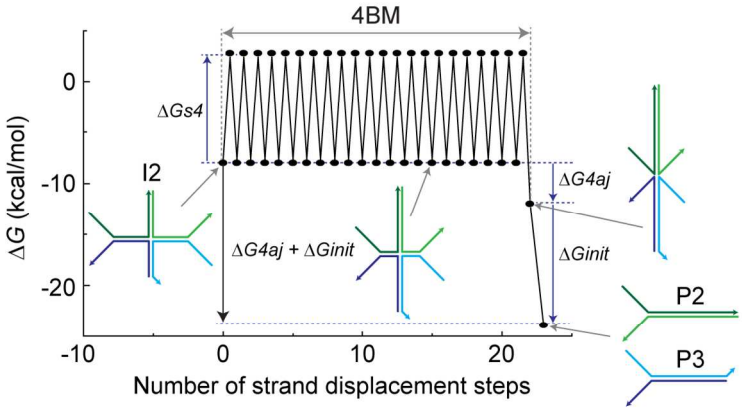

Figure S2C. The detailed IEL for step III. The thermodynamic driving force is an entropy gain and the elimination of four-arm junction point in I2.

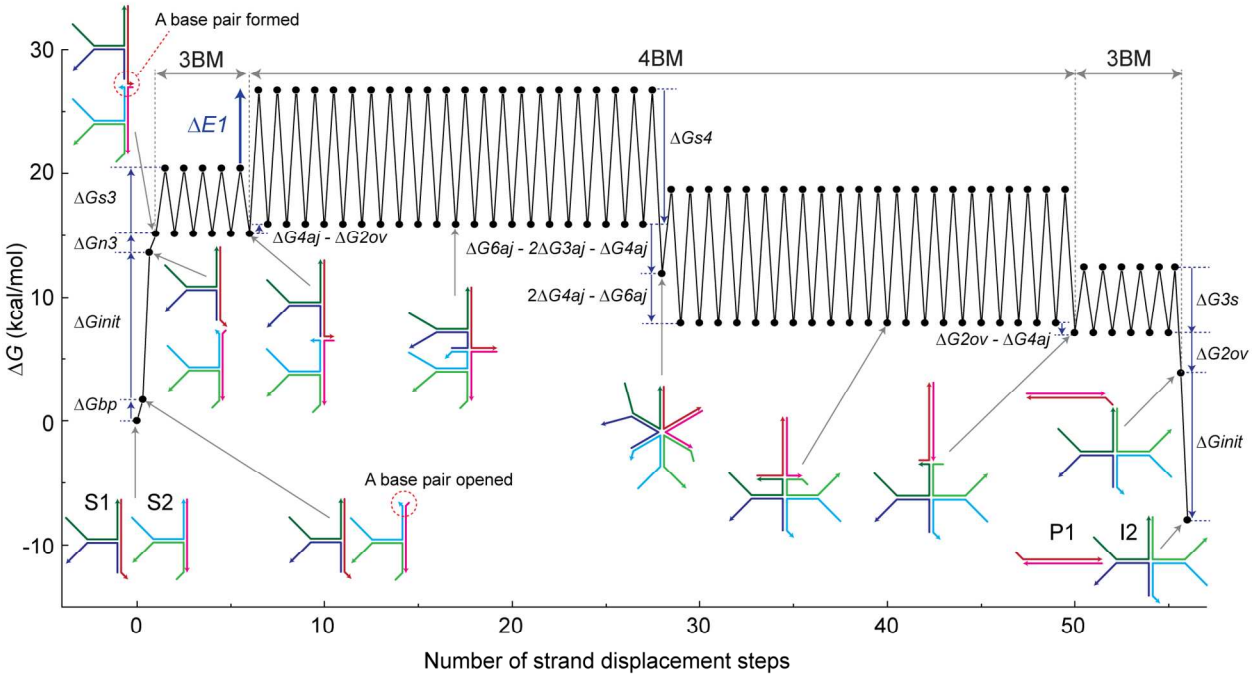

Figure S2D. The detailed IEL for the leakage reaction. The thermodynamic driving force is the same as the overall catalytic reaction. Because of the existence of the energy barrier $\Delta E1$, at the transition between the three-way branch migration and the four-way branch migration, the branch migration is strongly biased backwards. The last step of the leakage reaction, where I2 is converted into P2 and P3 (Figure S1C) is exactly the same as the step III (Figure S2C), thus not shown.

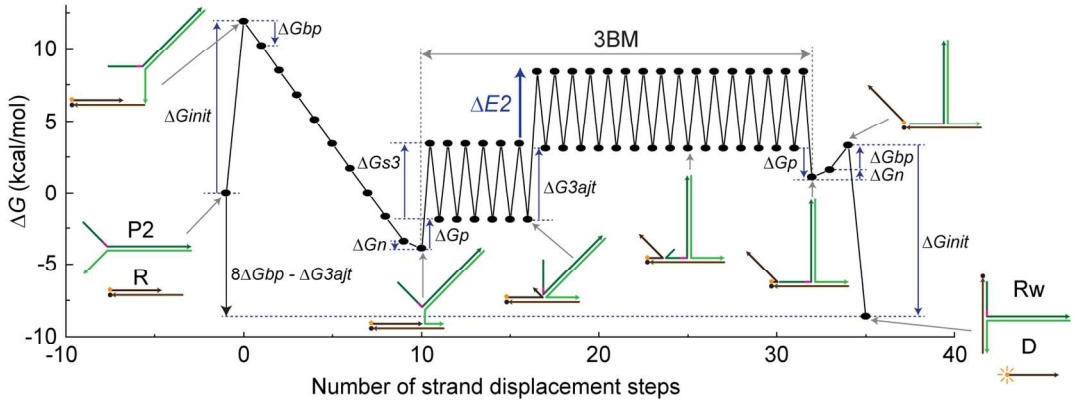

Figure S2E. The detailed IEL for the reporting reaction. The thermodynamic driving force is the gain of 8 bp against the formation of the three-arm junction point with the T2 bulge in Rw. Because of the existence of the energy barrier $\Delta E2$ at the transition from no three-arm junction to one three-arm junction, the branch migration will be strongly biased backwards, which requires a longer toehold.

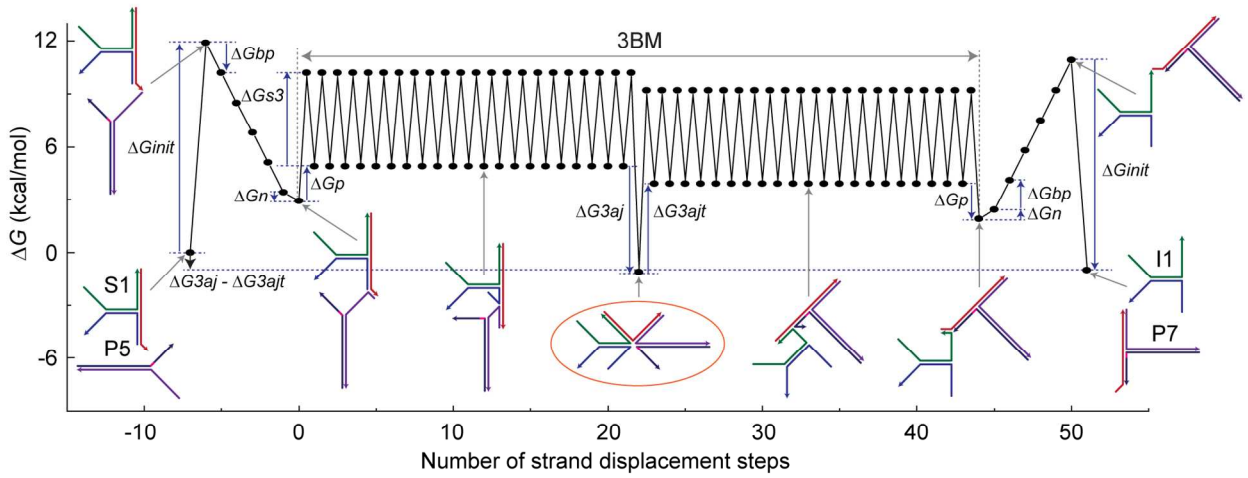

Figure S2F. The detailed IEL for step I for an output catalyst without a low-energy intermediate. The thermodynamic driving force is the formation of the three-arm junction in P7 with the T2 bulge, by eliminating the three-arm junction point in S1 without a bulge. Note that there exists a low energy reaction intermediate without any junction (circled in orange). Due to the low energy of this intermediate, a deep-well can be seen at the IEL. Thus, it can be expected that the system spends certain time at this intermediate. This might be the reason why the reaction kinetics for P5 was slower than the single-stranded catalyst C1 (Figure S9F). Another possibility is the presence of a sawtooth with a higher step height before or after the formation of the stable intermediate.

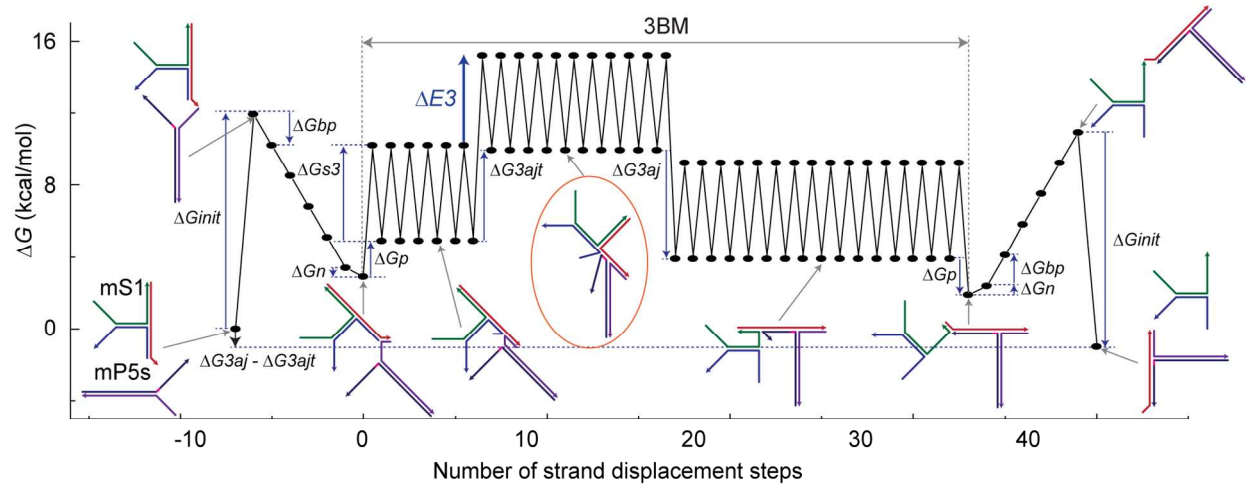

Figure S2G. The detailed IEL of step I for an output catalyst with a high energy intermediate. The thermodynamic driving force is the same as Figure S2F. However, in contrast with Figure S2F, the system will experience the energy barrier $\Delta E3$ during the shift from one three-arm junction in the system

to two three-arm junctions in the system (circled in orange). Because of the existence of this energy barrier, the branch migration will be strongly biased backward. When an associative toehold is applied to a hairpin system, as in the original research,[3] the IEL of the reaction will be similar to this case. In contrast with others IELs, the IEL here was drawn based on the 16 nt specificity domain to agree with the experiment (Figure S9B).

S3. Calculation of rate constants and kinetic simulation for three-arm junction substrates

The catalytic rate constant k_{cat} – A single-layer catalytic reaction with three-arm junction substrates can be modeled as:

$$\mathrm{S1} + \mathrm{S2} + \mathrm{C1} \xrightarrow{k_{cat}} \mathrm{P1} + \mathrm{P2} + \mathrm{P3} + \mathrm{C1} \quad (1)$$

Leakage can initially be ignored because it is orders of magnitude slower than the catalytic reaction. Therefore, the rate equation of P2 can be derived from equation (1) as:

$$d[\mathrm{P2}] / dt = k_{cat} [\mathrm{S1}] [\mathrm{S2}] [\mathrm{C1}] \quad (2)$$

When the initial condition is $[\mathrm{S1}]_0 = [\mathrm{S2}]_0$, $[\mathrm{C1}]_0$, the mass balance equations are:

$$[\mathrm{S1}] = [\mathrm{S2}] \quad (3)$$

$$[\mathrm{P2}] = [\mathrm{S1}]_0 - [\mathrm{S1}] \quad (4)$$

$$[\mathrm{C1}] = [\mathrm{C1}]_0 \quad (5)$$

Insertion of equations (3) through (5) into (2), and following integration yields:

$$[\mathrm{P2}] = (k_{cat} [\mathrm{S1}]_0^2 [\mathrm{C1}]_0 t) / (1 + k_{cat} [\mathrm{S1}]_0 [\mathrm{C1}]_0 t) \quad (6)$$

The delay of the reporting reaction between P2 and R was not considered here, because the reporting reaction is much faster than the catalytic reaction.[17] This allows one to consider the fluorescence signal as a direct measurement of the P2 concentration. Therefore, equation (6) was fit to the 500 pM trace (Figure S3A), yielding $k_{cat} = 2.84 \cdot 10^{13}$ $M^{-2}s^{-1}$. The inset shows that the initial portion of the reaction does not fit well due to the initial transient delay. The source of the transient delay occurs during reaction step **III** (Figure S1B, S2C), which is the unimolecular reaction through four-way branch migration. A similar initial transient delay was observed for a kissing loop catalytic substrate,[18] which also has four-way branch migration at the last step of the catalytic reaction. The reaction step **III** eventually becomes the rate-limiting step at higher catalytic concentrations. In fact, the data shows no difference of the reaction speed among 5, 10, and 50 nM catalysts (Figure S3B). Also, even at lower catalytic concentrations, the influence of this unimolecular reaction becomes stronger as the catalyst concentration becomes higher and the overall reaction speed approaches its saturated speed. This is a reason for the poor fitting to the 1 nM catalytic reaction (Figure S3C). Therefore, $k_{cat} = 2.84 \cdot 10^{13}$ $M^{-2}s^{-1}$ should be considered as the rate constant when a bimolecular reaction between a catalyst and a substrate is the rate limiting step of the overall catalytic reaction. The k_{cat} of a linear substrate for the entropy-driven system was adapted from the

literature where the same analytical method was used.[17] The k_{cat} of a hairpin substrate was calculated from enzymatically synthesized CHA,[19] where k_{app} was defined as the apparent rate constant including the contribution of the hairpin eA_1. Therefore, $k_{app} = k_{cat}$ [eA_1], where k_{app} = 0.17 $nM^{-1}h^{-1}$ and [eA_1] was assumed to be the initial concentration, 100 nM.

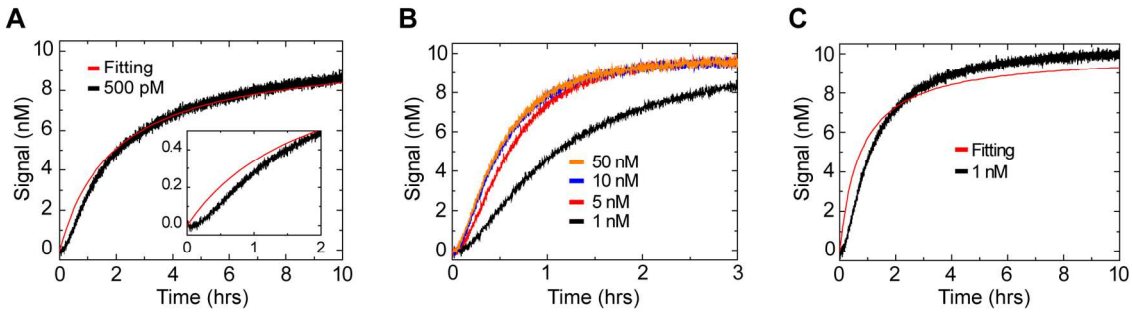

Figure S3. Catalytic rate constants for three-arm junction substrates. The fluorescence intensity was normalized so that 10 nM corresponds to the maximum fluorescence intensity and 0 nM corresponds to the initial fluorescence intensity for each kinetic trace. [S1] = [S2] = 10 nM, [R] = 20 nM. **(A)** The kinetic trace with 500 pM of catalyst C1 was fit to equation (6), and $k_{cat} = 2.84 \cdot 10^{13}$ $M^{-2}s^{-1}$ was extracted. The inset shows the deviation of the fitting trace from the kinetic trace due to the initial transient. **(B)** Kinetic traces with different concentrations of the catalyst C1. **(C)** The kinetic trace with 1 nM catalyst C1 was fit to equation (6). Although $k_{cat} = 3.71 \cdot 10^{13}$ $M^{-2}s^{-1}$ was extracted, the result was not included in Table 1 because it yielded a worse fit.

The leakage rate constant k_{leak} – A leakage reaction of three-arm junction substrates was modeled as following:

$$S1 + S2 \xrightarrow{k_{leak1}} P1 + P2 + P3 \quad (7)$$

The rate equation of P2 can be derived from equation (7) as:

$$d[P2] / dt = k_{leak1} [S1] [S2] \quad (8)$$

In order to convert a fluorescence intensity into a molecular concentration of the leakage at high concentrations used in Figure 2D, it was necessary to consider the influence of the 2 nt deletion at the domain d1s (the 5' ends of the domain d1 was deleted). The 2 nt was initially deleted in order to reduce the background signal from R + S1. However, the deletion leaves 2 nt exposed on the reporting waste Rw, which allows the backward reaction of the reporting reaction by forming a Rw-D complex (Figure S4A). The elimination of the three-arm junction in Rw also facilitates the reaction. NUPACK[20] was used to predict the population of Rw-D complexes, and the population was 0 % at 10 nM (the experimental condition in Figure 2C), but increased to 18 % at 500 nM (the experimental condition in Figure 2D). Similar to this prediction, although the maximum fluorescence intensity for R + S1 + S2 reaction was 11 a.

u. at 10 nM, it was only 399 a. u. at 500 nM (Figure S4B). The difference between NUPACK prediction and experimental result could be due to the inaccuracy of the energy parameter of the three-arm junction and the presence of the Dye-Quencher pair interaction.[21] Because of this non-linearity between the fluorescence intensity and the concentration, the maximum fluorescence intensity of the leakage at 500 nM substrates concentration was not used to normalize the data. Instead, it can be seen that the fluorescence intensity of the 500 nM leakage reaction before the addition of excess catalysts is the same range of the maximum fluoresce intensity of the 10 nM reaction (Figure S4B, inset). Consequently, it is appropriate to convert fluorescence intensities of the leakage reaction into concentrations based on the 10 nM reaction. Therefore, after subtracting the background (R + S1) from the leakage (R + S1 + S2), the leakage at 500 nM substrate concentration was normalized with the final intensity at 10 nM substrate concentration (Figure S4C). In order to avoid the influence of the initial leakage, the kinetic trace from 20 to 30 hours was fit to equation (8) as the initial slope of the leakage reaction, and $k_{leak1} = 2.20 \cdot 10^{-2}$ $M^{-1}s^{-1}$ was extracted. Note that this time window can be considered as the initial portion of the leakage due to its long time scale. The k_{leak} of a linear substrate for the entropy-driven system was adapted from the literature where the same leakage model was applied.[17] The k_{leak} of a hairpin substrate was calculated from enzymatically synthesized CHA,[19] where k_{Asy} was defined as the apparent rate constant including the contribution of hairpin eA_1. Therefore, $k_{Asy} = k_{leak}$ $[eA_1]$, where $k_{Asy} = 0.84 \cdot 10^{-4}$ h^{-1} and $[eA_1]$ was assumed to be the initial concentration, 100 nM. In addition to CHA, hairpin chain reaction (HCR)[22] is one of the most widely used catalytic systems based on hairpin substrates. It can be expected that HCR has a smaller leakage rate than CHA considering their leakage pathway differences. Therefore, we cannot conclude that multi-arm junction substrates have better ratio of the catalytic rate constant to the leakage rate constant than HCR.

We also performed an experiment to estimate the reaction between R and the single-stranded output tails on S1 and S2, which does not require the formation of P2 by a leakage in order to increase a fluorescence intensity. For this purpose, two of single-stranded DNAs were designed (Figure S4D). ss1 has the same sequence of the output tail on S1 (domains d1s-T2), and ss2 has the same sequence of the output tail on S2 (domains d2-3). As expected from the reaction R + S1 (Figure 2D), R + ss1 showed a clear fluorescence increase. In addition, the larger fluorescence increase was observed when R, ss1, and ss2 were mixed together (R + ss1 + ss2), showing that those two single-stranded DNA molecules can cooperatively displace the D strand from R. Importantly, the result indicates that some portion of the observed leakage (Figure 2D) might be due to the reaction between R and the single-stranded output tails on the substrates (domains d1s-T2 of S1 and domains d2-3 of S2) with the same mechanism. Thus, the actual leakage modeled in equation (7) could be smaller than the calculation above. Consequently, we could not quantify the initial leakage by comparing the fluorescence intensity difference between R + S1 and R + S1 + S2 in Figure 2D, because the intensity difference might be due to this background signal.

We expect that this type of leakage will be suppressed easily by using clamps.[18] The stronger fluorescence intensity of R + ss1 + ss2 than R + S1 + S2 would be due to the steric hindrance exerted by the domain b on the substrates S1 and S2.

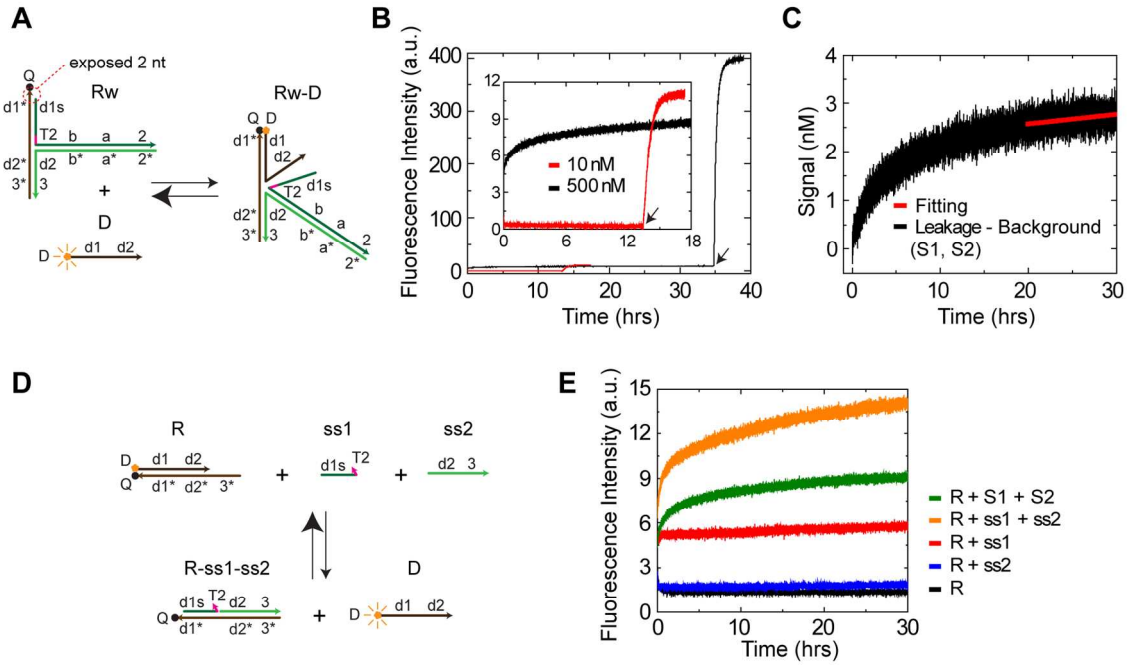

Figure S4. The leakage rate constant for three-arm junction substrates. (A) The binding of D with Rw was mediated by the exposed 2 nt at the 3' end of domain d1*. The reaction is negligible under a 10 nM concentration of each species, but was influential at higher concentrations. **(B)** Non-linearity of the maximum fluorescence intensity when the concentration was high. The maximum fluorescence intensity was 11 a. u. for the10 nM experiment, where [S1] = [S2] = 10 nM, [R] = 20 nM. However, the maximum fluorescence intensity was only 399 a.u. for the 500 nM experiment, where [S1] = [S2] = 500 nM, [R] = 700 nM. Note: the maximum fluorescence intensity would be 550 a.u. if the relationship between the fluorescence intensity and the concentration were linear. The fluorescence data is not normalized. Black arrows show the addition of the catalyst C1 to obtain the maximum fluorescence intensity. **(C)** The calculation of the leakage rate constant. The background reaction (R + S1) was subtracted from the leakage (R + S1 + S2) from Figure 2D at 500 nM, and the initial fluorescence intensity was adjusted to zero. Then, the fluorescence intensity was normalized using the average maximum fluorescence changes of the 10 nM concentration experiments in Figure 2C. Considering the slowness of the leakage, the time window before the addition of catalyst can be considered as the initial rate period. Therefore, the slope from 20 to 30 hours was fit to equation (8), and $k_{leak1} = 2.20 \cdot 10^{-2}$ $M^{-1}s^{-1}$ was extracted. **(D)** The experimental design to estimate the reaction between R and the single-stranded output tails on S1 and S2. ss1 is the output tail on S1, and ss2 is the output tail on S2. **(E)** Kinetic traces of the background

reactions. [S1] = [S2] = [ss1] = [ss2] = 500 nM, [R] = 700 nM. The traces of R and R + S1 + S2 are from Figure 2D.

Kinetic simulation – Equation (1) is a simplified catalytic reaction model, which is useful to compare the overall performance of different systems. However, in order to accurately simulate the reaction kinetics, the reaction must be dissected into individual steps based on Figures 2A and 2B.

$$\mathrm{S1} + \mathrm{S2} \xrightarrow{k_{leak1}} \mathrm{P1} + \mathrm{P2} + \mathrm{P3} \tag{9}$$

$$\mathrm{C1} + \mathrm{S1} \underset{k_{-1}}{\overset{k_1}{\rightleftharpoons}} \mathrm{P1} + \mathrm{I1} \tag{10}$$

$$\mathrm{I1} + \mathrm{S2} \underset{k_{-2}}{\overset{k_2}{\rightleftharpoons}} \mathrm{I2} + \mathrm{C1} \tag{11}$$

$$\mathrm{I2} \xrightarrow{k_3} \mathrm{P2} + \mathrm{P3} \tag{12}$$

$$\mathrm{P2} + \mathrm{R} \xrightarrow{k_4} \mathrm{Rw} + \mathrm{D} \tag{13}$$

Although C1 and P3 can hybridize using toehold domain 1, the reaction was not important in our system if the dissociation rate constant was larger than 10^{-2} s^{-1}, which was used in the literature.[23] The rate constants adopted for our simulations are $k_1 = k_2 = 5 \cdot 10^5$ $M^{-1}s^{-1}$ and also reflect a typical value in the literature for toehold exchange reactions.[8] The backward reaction of equation (10) involves the formation of a three-arm junction, whose energy penalty is around 5 kcal/mol. An equivalent energy penalty by a mismatch base pair is known to slow down toehold-mediated strand reactions by 2 to 3 orders of magnitude.[16] Therefore, k_{-1} was assumed to be slow with a value of $1 \cdot 10^3$ $M^{-1}s^{-1}$. During the process of simulation, we realized that the backward reaction of equation (11) has to be significantly slower than its forward reaction in order to reproduce the experimental data. A reason for this is because the strand displacement reaction is difficult between the isoenergetic forms I2 and C1 (Figure S5).

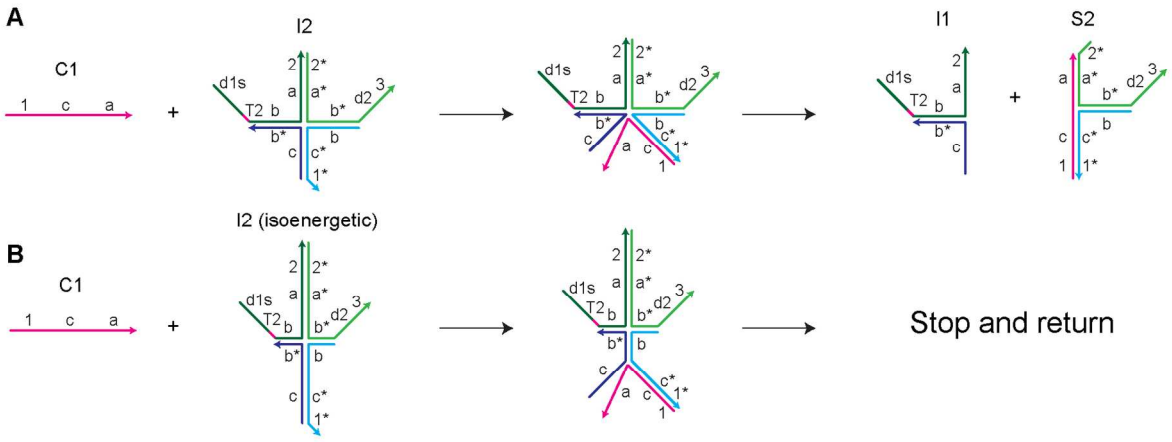

Figure S5. C1 cannot complete strand displacement reaction with isoenergetic form of I2. (A) C1 can complete strand displacement with I2 if domains c and a in I2 are connected each other. **(B)** C1

cannot complete strand displacement with isoenergetic forms of I2 if domain c and a in I2 are separated by domain b. As a result, C1 will continue branch migration backwards and then dissociate from I2.

Here, C1 can complete strand displacement with the appropriate form of I2 (Figure S5A). In contrast, when C1 tries to perform strand displacement with other isoenergetic forms of I2 (Figure S5B), the reaction will be stopped by the domain b of I2, which separates domains a and c. Because four-way branch migration is slow (step time ~ 1s)[9] and three-way branch migration is fast (step time ~ 100 μs)[8], I2 is assumed to be static after C1 initiates strand displacement. Therefore, the available population of I2 for strand displacement (Figure S5A) is 1/(length of domain b), which is 1/22. As a result, $k_{-2} = k_2 /22$, which is ~$2 \cdot 10^4$ $M^{-1}s^{-1}$. k_3 in equation (12) is the rate constant of four-way branch migration with 22 nt, which is assumed to be $1 \cdot 10^{-3}$ s^{-1} based on the literature from a similar design.[10] k_4 in equation (13) was assumed to be $1 \cdot 10^6$ $M^{-1}s^{-1}$, which is a typical value for strand displacement with a long toehold.[1]

In addition to equations (9) through (13), it was necessary to consider the low catalytic turnover observed. One possible reason for low catalytic turnover is defective DNA strands, which was suggested by Zhang *et al*.[23] The authors reasoned that toehold exchange reactions are sensitive to a few defects in the invader strands. For their entropy-driven system, the Fuel strand was assumed to contain such defects,[23] which corresponds to C1 and I1 for our three-arm junction substrates. Therefore, we hypothesized the existence of defect-substrates here (Figure S6).

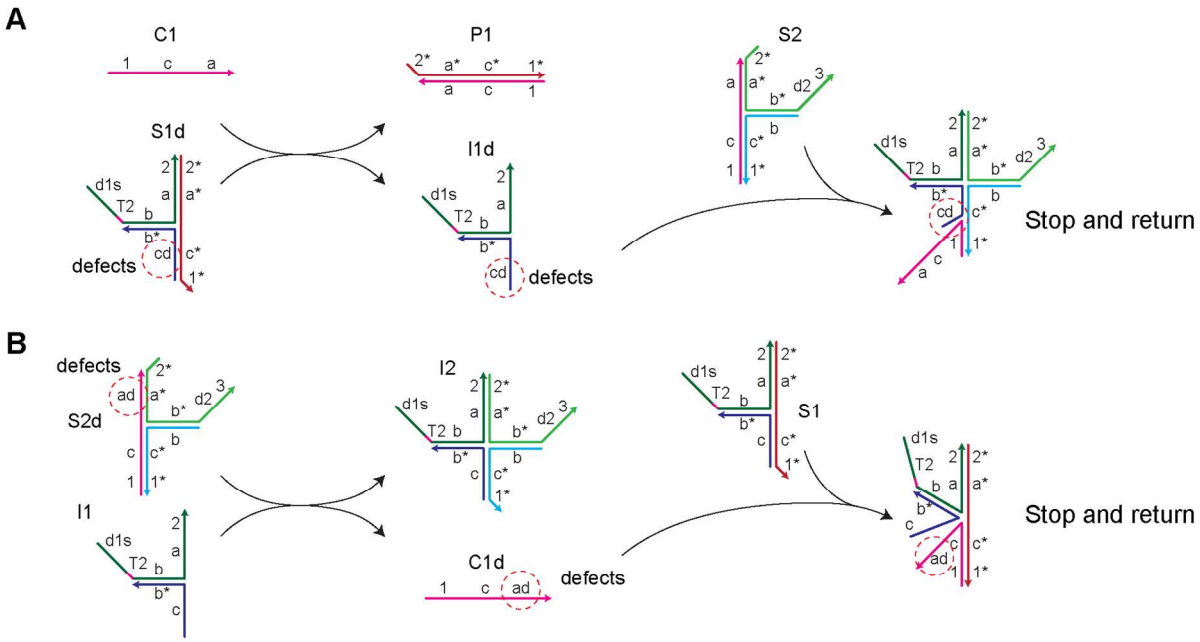

Figure S6. Low catalytic turnover caused by defects of DNA strands. (A) Defect-substrate S1d produces defect-intermediate I1d, which is unable to perform strand displacement with S2. **(B)** Defect-substrate S2d produces defect-catalyst C1d, which is unable to perform strand displacement with

S1.

For instance, if the defect-substrate S1d has significant sequence defects at domain c (shown as domain cd in Figure S6A), the reaction with C1 will produce defect-intermediate I1d. Since I1d also has sequence defects, it is unable to react with substrate S2 to displace a defect-free catalyst C1 (pink strand in S2) for the next round of reaction. As a result, S1d consumes C1 and poisons the catalytic reaction. Similarly, defect-substrate S2d will consume I1 and produce defect-catalyst C1d, which is unable to perform strand displacement with substrate S1. Although there are multiple scenarios to lower the catalytic turnover, we used this hypothetical model here. Based on Figure S6, the following equations can be made.

$$\mathrm{C1} + \mathrm{S1d} \xrightarrow{k_1} \mathrm{P1} + \mathrm{I1d} \tag{14}$$

$$\mathrm{I1} + \mathrm{S2d} \xrightarrow{k_2} \mathrm{I2} + \mathrm{C1d} \tag{15}$$

In addition to ignoring the reaction between C1 and P3, we also ignored the reactions of I1d with P1 or S2, and the reactions of C1d with I2 or S1, with the assumption that those reactions will only temporary form a complex and then quickly dissociate into their reactants. The forward rate constants for equations (14) and (15) were assumed to be the same as equations (10) and (11), and the defect population of S1d and S2d was adjusted to be 2 % each.

Finally, in order to account for the initial leakage with a ~10 hour time scale (Figure S4C), we hypothesized the existence of substrates with initial leakage S1i and S2i as below.

$$\mathrm{S1i} + \mathrm{S2i} \xrightarrow{k_i} \mathrm{P1} + \mathrm{P2} + \mathrm{P3} \tag{16}$$

The rate constant k_i and population of S1i and S2i were adjusted for experimental data as $k_i = 5 \cdot 10^4$ $M^{-1}s^{-1}$ and 0.46 % each. The simulation result using equations (9) through (16) is in Figure S7A, and agrees well with experimental data and reproduced the observed saturation of reaction speed at high concentration of catalyst. This result supports the proposed reaction model. Figure S7B shows the leakage reaction in Figure S4C. The agreement is satisfactory, but we would like to note that the observed leakage might be the reaction caused by the reaction between R and the single-stranded output tails on S1 and S2 (Figure S4D, E), which is different from the additive of equations (9) and (16).

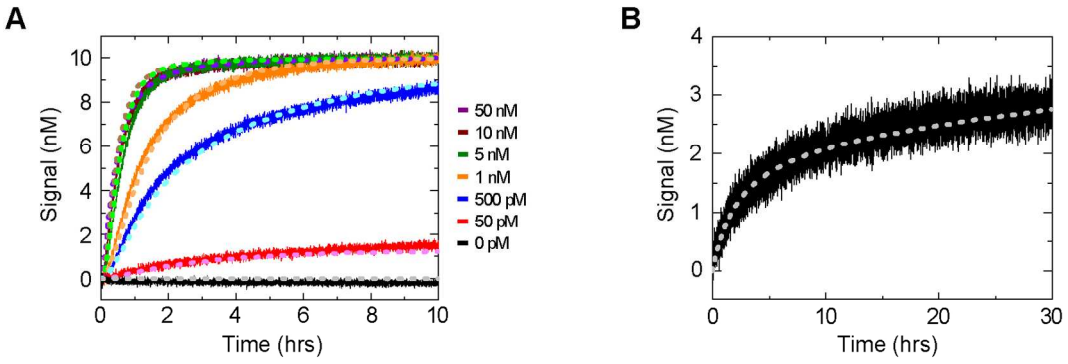

Figure S7. Kinetic simulation for single-layer catalytic system with three-arm junction substrate. **(A)** 10 nM concentration of substrates with different concentrations of catalyst. Kinetic simulations are shown as dots with weak colors. The data is the combination of Figure 2C and Figure S3B. **(B)** Leakage reaction at 500 nM concentration of substrates, using data of Figure S4C.

S4. Single-layer catalytic system with three-arm junction substrates based on 16nt specificity domains

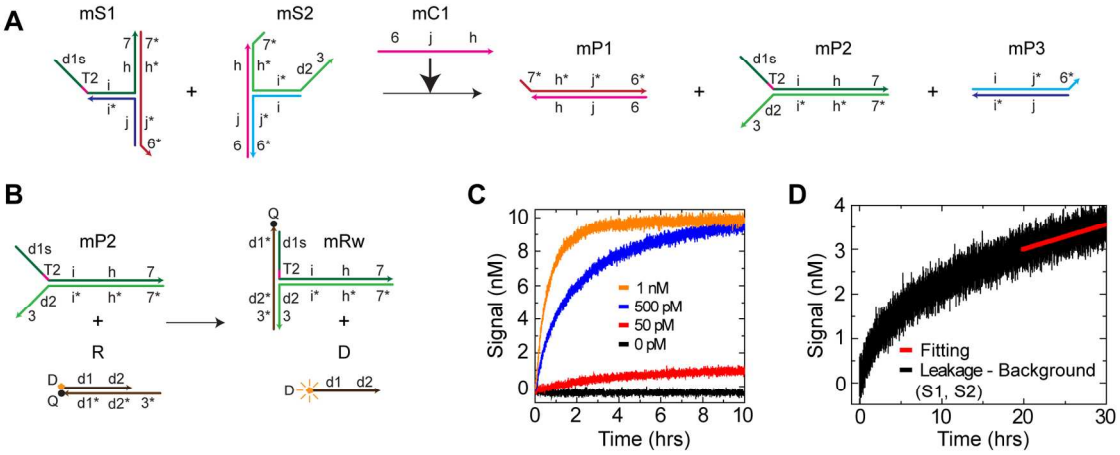

Figure S8. Single-layer catalytic system with three-arm junction substrates based on 16 nt specific domains. **(A)** A simplified schematic of the catalytic pathway. The detailed catalytic pathway is as same as Figure 2A with the exception of domains. **(B)** The reporting reaction. **(C)** Kinetic traces with different concentrations of the catalyst mC1. The fluorescence intensity was normalized so that 10 nM corresponds to the maximum fluorescence intensity and 0 nM corresponds to the initial intensity. [mS1] = [mS2] = 10 nM, [R] = 20 nM. **(D)** The calculation of the leakage rate constant. The background reaction (R + mS1) was subtracted from the leakage (R + mS1 + mS2) at 500 nM, and the initial fluorescence intensity was adjusted to zero. Then, the fluorescence intensity was normalized using the average maximum fluorescence changes of the 10 nM concentration experiments in Figure S8C. Finally, the slope from 20 to 30 hours was fit to equation (8), and $k_{leak} = 6.61 \cdot 10^{-2}$ $M^{-1}s^{-1}$ was extracted.

S5. Design considerations of output formation

In order to construct DNA cascade systems, it is necessary for an output from one layer to smoothly trigger downstream layers with a catalyst. In the case of multi-arm junction substrates, outputs are formed via associative toeholds[3] with junction positions being able to be varied, which in turn affects the reaction kinetics. Therefore, two different positions of a junction were tested with three-arm junction substrates

based on 16 nt specificity domains (Figure S9A). For the first set, the junction position was between domain j1 and j2 (mP5s-t), with a variation having T2 bulge (mP5s). The T2 bulge was used because it was shown to speed up the associate toehold reaction speeds by stabilizing a three-arm junction point.[3] The second set has the junction between domains j2 and h (mP5-t), with a variation having a T2 bulge (mP5). The consequence of the different junction positions can be seen on their reaction kinetics (Figure S9B). Comparing with the single-stranded catalyst mC1, the reaction of mP5s-t was significantly slower, even after the addition of the T2 bulge (mP5s). One interesting result is the relative quickness of the reactions when compared to hairpin substrates.[3] This could be due to the difference of the junction position, sequence, or the fundamental difference of the mechanism of strand displacement for hairpins. In comparison, the reaction speed of mP5-t was already similar to mP5s, and the addition of theT2 bulge (mP5) resulted in the same speed as mC1. Because the stoichiometry concentration of the substrates and catalysts (5 nM) were used here, the reaction speeds of mC1 and mP5 were likely limited by the unimolecular reaction step **III**, as shown in Figure S3B. Nonetheless, the results showed the best design to be mP5. As such, this design was applied for all other experiments. The reason of the slow reaction speed of mP5s or mP5s-t can be explained using the IEL (Figure S2G). We have not tested a junction position between domain 6 and j1 for an output catalyst, because it results in the domains j-h to be exposed on a substrate all the time and become the source of leakage.

When the mP5 design is applied, one thing to be considered is that a toehold and its neighboring specificity domains will be exposed together on a substrate initially. As an example, two types of substrates were examined for feed forward catalytic systems (Figure S9C). Here, mS3 has the domain j2 covered, but mS3u has the domain j completely exposed (domain j = j1 + j2). NUAPCK[20] predicted that only 12 % of mS1 and mS3 form a complex at 10 nM, because the formation of mS1-mS3 complex needs to form a five-arm junction in order to maintain the maximum number of base pairs. In comparison, 75% of mS1 and mS3u were predicted to form a complex at 10 nM, because the formation of mS1-mS3u complex can eliminate the three-arm junction point in mS1. Those predictions agreed with the PAGE result, which showed that (mS1 + mS3u) has a larger mobility shift than (mS1 + mS3), indicating the formation of a stable mS1-mS3u complex (Figure S9D). This type of complex formation can be expected to sequester the toehold domain 6* of the substrate mS1. Therefore, the design of mS3 was applied to all other experiments.

Reaction speed differences between a single-stranded catalyst and a junction catalyst was also tested for three-arm junction substrates with 22 nt specificity domains (Figure S9E) and four-arm junction substrates with extended toeholds (Figure S9G). Three-arm junctions with 6 nt toehold showed approximately a three times slowness of the overall reaction (estimated from the initial slopes) for the junction catalyst P5 than the single-stranded catalyst C1 (Figure S9F). Nonetheless, this reaction is quick enough to construct signal cascade systems based on the toehold exchange reaction.[8] In four-arm junction

substrates, the extended 8 nt toehold domain 1 enabled the same overall reaction speed between the single-stranded catalyst C1x and the junction catalyst P8au (Figure S9H). Therefore, extended toehold domain 1 can speed up the reaction for three-arm junction substrates. The relative slowness of the reactions in Figure S9H, comparing with Figure S9F or Figure S16E, is likely due to the poor quality of unpurified DNA strands used here.

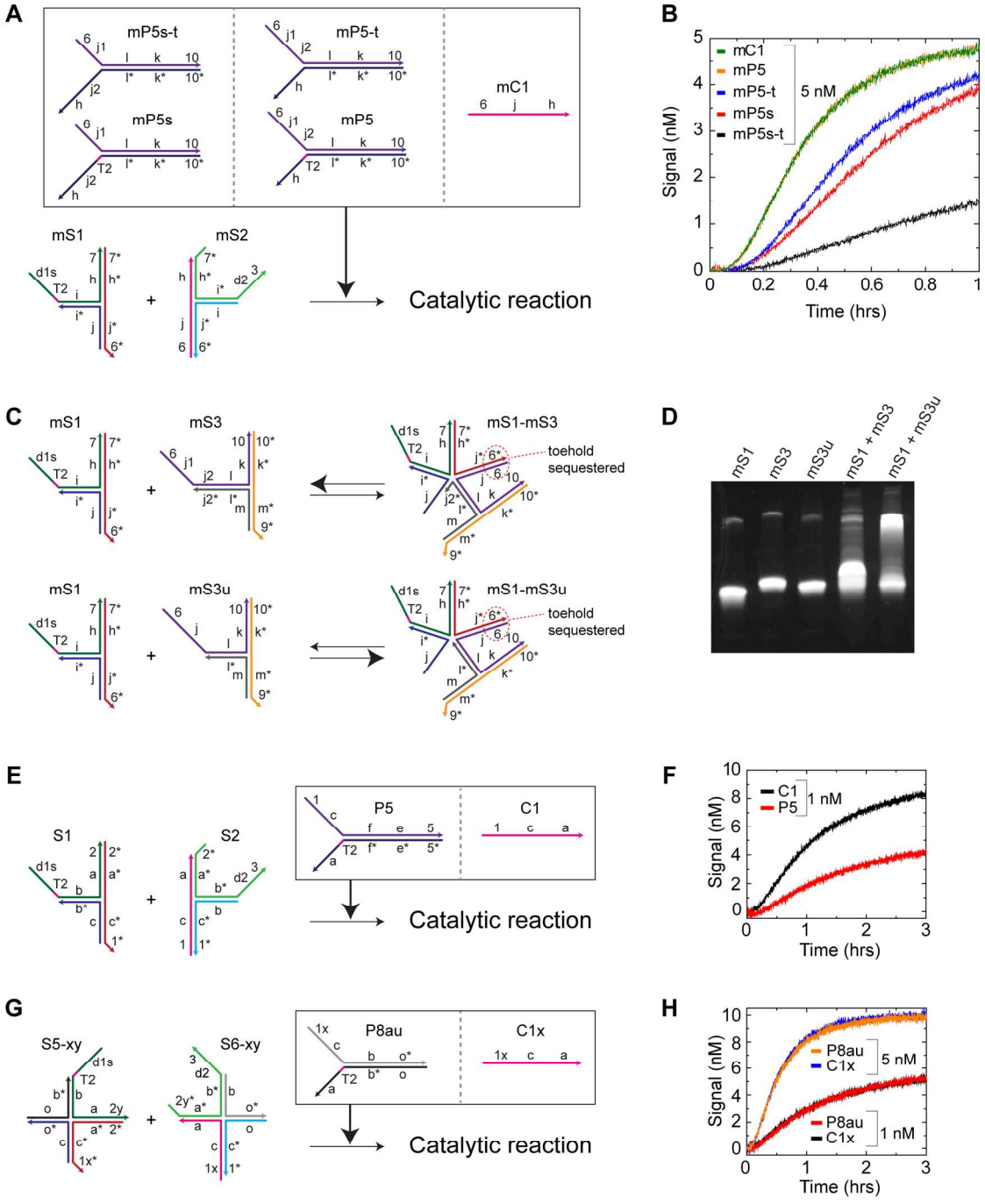

Figure S9. Design consideration for output signal formation. (A) Different catalyst designs were tested for single-layer catalytic systems with three-arm junction substrates based on 16 nt specificity domain length. Domain j = domains j1 + j2. The reporting reaction is the same as Figure S8B. **(B)** Kinetic traces with different catalyst species. [mS1] = [mS2] = 5 nM, [R] = 10 nM. Unpurified DNA strands were used here. **(C)** Comparison of complex formations between mS1-mS3 and mS1-mS3u. While the 6-j domains of mS3u are completely exposed, the j2 of mS3 are covered. **(D)** 10 % native PAGE analysis of the complex formation. 10 μL of 0.5 μM DNA solution was used on each lane and stained with dye. mS1 + mS3 showed a small shift during gel migration, indicating that their interaction was weak. In comparison, mS1 + mS3u showed a large shift during gel migration, indicating a stronger interaction. Unpurified DNA strands were used. **(E)** Different catalyst designs were tested for single-layer catalytic systems with three-arm junction substrates based on 22 nt specificity domain length. **(F)** Kinetic traces with different catalyst species. [S1] = [S2] = 10 nM, [R] = 20 nM. **(G)** Different catalyst designs were tested for a single-layer catalytic system with four-arm junction substrates. **(H)** Kinetic traces with different catalyst species. [S5xy] = [S6xy] = 10 nM, [R] = 20 nM. Unpurified DNA strands were used here.

S6. Detailed reaction schematic and kinetic simulation of two-layer feed forward catalytic system with three-arm junction substrates

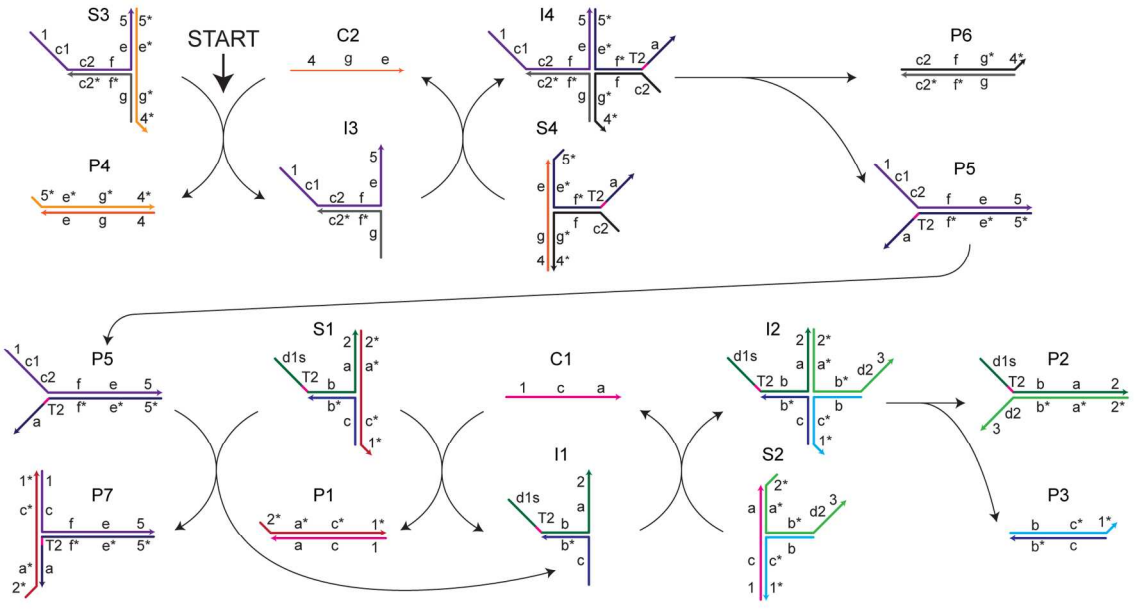

Figure S10. Detailed reaction schematic of two-layer feed forward catalytic system with three-arm junction substrates. A schematic of the catalytic pathway. The pathway starts with the reaction between the substrate S3 and the catalyst C2. After one cycle of the catalytic reaction, the first layer produces the

product P5, whose single-stranded sequence has the same domains as the catalyst C1 for the second layer. Domain c = domain c1 + c2. The reporting reaction is the same as the single-layer catalytic system (Figure 2), thus not shown.

Based on Figure S10, the following equations can be made.

$$\mathrm{S3} + \mathrm{S4} \xrightarrow{k_{leak1}} \mathrm{P4} + \mathrm{P5} + \mathrm{P6} \tag{17}$$

$$\mathrm{C2} + \mathrm{S3} \underset{k_{-5}}{\overset{k_5}{\rightleftharpoons}} \mathrm{P4} + \mathrm{I3} \tag{18}$$

$$\mathrm{I3} + \mathrm{S4} \underset{k_{-6}}{\overset{k_6}{\rightleftharpoons}} \mathrm{I4} + \mathrm{C2} \tag{19}$$

$$\mathrm{I4} \xrightarrow{k_7} \mathrm{P5} + \mathrm{P6} \tag{20}$$

$$\mathrm{P5} + \mathrm{S1} \underset{k_{-8}}{\overset{k_8}{\rightleftharpoons}} \mathrm{P7} + \mathrm{I1} \tag{21}$$

$$\mathrm{P5} + \mathrm{S1d} \xrightarrow{k_8} \mathrm{P7} + \mathrm{I1d} \tag{22}$$

$$\mathrm{C2} + \mathrm{S3d} \xrightarrow{k_5} \mathrm{P4} + \mathrm{I3d} \tag{23}$$

$$\mathrm{I3} + \mathrm{S4d} \xrightarrow{k_6} \mathrm{I4} + \mathrm{C2d} \tag{24}$$

$$\mathrm{S3i} + \mathrm{S4i} \xrightarrow{k_i} \mathrm{P4} + \mathrm{P5} + \mathrm{P6} \tag{25}$$

The leakage rate constant of equation (17) was assumed to be the same as equation (9). The rate constants used were $k_{-5} = k_{-1}$, $k_{-6} = k_{-2}$, and $k_7 = k_3$. Since we observed a slow feed forward system, the forward rate constants were adjusted to be $k_5 = k_1/2$ and $k_6 = k_2/2$. For equation (21), with output catalyst P5, the rate constants were adjusted to be $k_8 = k_{-8} = 5 \cdot 10^4$ $M^{-1}s^{-1}$, which is ten times slower than the reaction of the single-stranded catalyst C1 in equation (10). The simulation result for the single-layer catalytic system, with the P5 input, is shown in Figure S11A, and the simulation agrees well with 5 nM P5. However, at 1 nM P5, the simulation agrees with the data only for the first hour, afterwards the deviation becomes large. One reason for the deviation is that the accumulation of product P7, produced by the reaction between P5 and S1, may inhibit the overall catalytic reaction. A second reason is that there could be side reactions. Regardless, we are unsure how to accurately model this reaction. Therefore, instead of introducing further hypothetical reactions, we acknowledge that our understanding of the system is not complete. A complete understanding requires measuring the kinetics of the individual reactions to predict the overall kinetics of the system. While this is clearly beneficial and is currently being consideration, it is beyond the scope of this manuscript to perform these experiments. The simulation for the two-layer feed forward system is shown in Figure S11B by combining equations (9) through (25). Here, the concentration of P5, due to initial leakage[1], was adjusted to 1 pM. This value is much smaller than the linear substrate from Zhang *et al.*, where the initial leakage was assumed to be much larger for the 10 nM substrate concetration.[1] A possible explanation is the difference of the leakage

mechanism between linear and multi-arm junction substrates. For linear substrates, leakage proceeds though three-way branch migration. As a result, initial leakage is expected to be instantaneous and the majority of malformed substrates will quickly decay into their products. In contrast, leakage proceeds through four-way branch migration for multi-arm junction substrates. As a result, the majority of the malformed substrates will decay slowly, which may cause a slow initial leakage (Figure S7B, first ~ 10 hours). S3d and S4d were adjusted to have a 3 % defect rate, while S3i and S4i were adjusted to have a 0.46 % defect rate. Although 100 pM, 1 pM, and 0 pM catalyst reactions agree well to our simulation, the 10 pM catalysis reaction does not agree (Figure S11B).

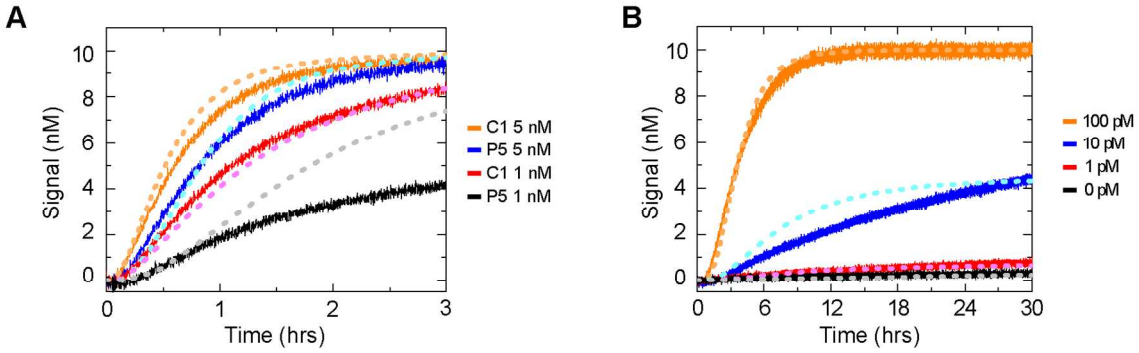

Figure S11. Kinetic simulation for two-layer feed forward catalytic system with three-arm junction substrate. (A) Simulation for data in Figure S9F, where single-stranded catalyst C1 and junction catalyst P5 were used as input catalyst for single-layer catalytic system with substrates S1 and S2. Kinetic simulations are shown as dots with weak colors. **(B)** Simulation for the two-layer feed forward system in Figure 3B.

S7. Detailed reaction schematic and kinetic simulation of cross-catalytic system with three-arm junction substrates

In the cross-catalytic system, the first layer is the same as the two-layer feed forward system (Figure S10). However, the product of the second layer, P3cr, has the catalytic domains 4-g-e in order to feedback to the first layer (Figure S12A). The reporter is the same with our other experiments (Figure S12B). Based on Figure S12A, B, the following equations can be made.

$$\mathrm{S1cr} + \mathrm{S2cr} \xrightarrow{k_{leak1}} \mathrm{P1} + \mathrm{P2cr} + \mathrm{P3cr} \tag{26}$$

$$\mathrm{C1} + \mathrm{S1cr} \underset{k_{-1}}{\overset{k_1}{\rightleftharpoons}} \mathrm{P1} + \mathrm{I1cr} \tag{27}$$

$$\mathrm{I1cr} + \mathrm{S2cr} \underset{k_{-2}}{\overset{k_2}{\rightleftharpoons}} \mathrm{I2cr} + \mathrm{C1} \tag{28}$$

$$\mathrm{I2cr} \xrightarrow{k_3} \mathrm{P2cr} + \mathrm{P3cr} \tag{29}$$

$$\mathrm{P3cr} + \mathrm{S3} \underset{k_{-9}}{\overset{k_9}{\rightleftharpoons}} \mathrm{P8cr} + \mathrm{I3} \tag{30}$$

$$\mathrm{P3cr} + \mathrm{S3d} \xrightarrow{k_9} \mathrm{P8cr} + \mathrm{I3d} \tag{31}$$

$$\mathrm{P2cr} + \mathrm{R} \xrightarrow{k_4} \mathrm{Rwcr} + \mathrm{D} \tag{32}$$

$$\mathrm{C1} + \mathrm{S1crd} \xrightarrow{k_1} \mathrm{P1} + \mathrm{I1crd} \tag{33}$$

$$\mathrm{I1cr} + \mathrm{S2crd} \xrightarrow{k_2} \mathrm{I2cr} + \mathrm{C1d} \tag{34}$$

$$\mathrm{S1cri} + \mathrm{S2cri} \xrightarrow{k_i} \mathrm{P1} + \mathrm{P2cr} + \mathrm{P3cr} \tag{35}$$

With the exception of equation (30) where the output catalyst P3cr reacts with the substrate S3, the reaction rate constants used were identical to the single-layer three-arm junction substrates in Section S3. Since a quick cross-catalytic system was observed, we used $k_9 = k_{-9} = 5 \cdot 10^5$ $M^{-1}s^{-1}$ in equation (30). This is ten times quicker than the reaction between P5 and S1, of which we do not have a reasonable explanation for the difference in the reaction speeds. The simulation and experimental data for the cross-catalytic system is shown in Figure S12C by combining equations (17) through (35). The population of defect-substrates and initial leakage substrates were assumed to be the same as the single-layer catalytic system so that S1crd and S2crd had a 2 % defect rate, and S1cri and S2cri had a 0.46 % defect rate. In order to account for the large leakage at 0 pM, the initial concentration of product P3cr was adjusted to be 70 pM. This large amount of P3cr did not reproduce the clear separation of the leakage and the 10 pM reaction. Again, further characterization of all individual reactions will be necessary to predict the overall kinetics of the system.

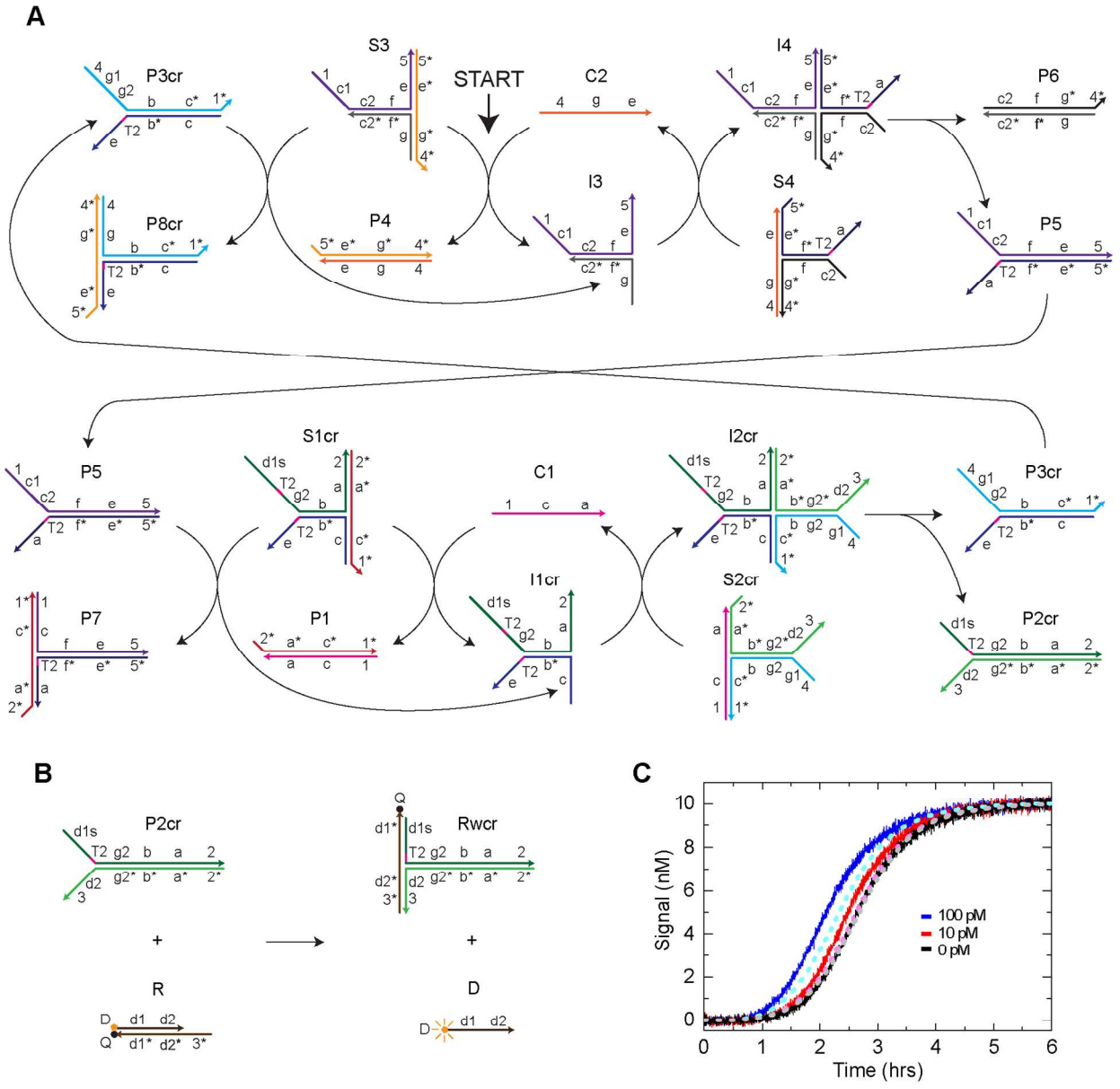

Figure S12. Detailed reaction schematic of cross-catalytic system with three-arm junction substrates. (A) A schematic of the catalytic pathway. The catalytic substrates in the first layer (S3, S4) are the same as substrates in two-layer feed forward catalytic system (Figure 3). The pathway starts with the reaction between the substrate S3 and the catalyst C2. After one cycle of the catalytic reaction, the first layer produces the product P5, whose single-stranded sequences have the same domain as the catalyst C1 for the second layer. The second layer then produces the product P3cr, whose single-stranded sequence have the same domain as the catalyst C2 for the first layer. Domain c = domains c1 + c2, and domain g = domains g1 + g2. **(B)** The reporting reaction. The reporter complex R is the same as all other experiments. **(C)** Kinetic traces with different concentrations of catalyst C2. [S1cr] = [S2cr] = [S3] = [S4]

= 10 nM, [R] = 20 nM. Kinetic simulations are shown as dots with weak colors.

S8. Background check of two-layer feed forward and cross-catalytic system with three-arm junction substrates

The leakage model in equation (7) considers only the reaction between S1 and S2, or other corresponding combinations of substrates. However, other leakage sources can appear if there exists design issues. To check this possibility, reaction components of feed forward and cross-catalytic systems were added step by step and their reaction kinetics were measured. For the feed forward catalytic system, an increase of the leakage was not observed by comparing the single-layer leakage (R + S1 + S2) with traces where other substrates were added, R + S1 + S2 + S3 and R + S1 + S2 + S4 (Figure S13A). Similarly, the cross-catalytic system showed no observable difference by comparing R + S1cr + S2cr with R + S1cr + S2cr + S3 and R + S1cr + S2cr + S4 (Figure S13B). Considering a very small value of k_{leak} and the fact that we have not performed any method to reduce initial leakage caused by malformed substrates,[1,19] those results indicate that a main source of leakage for feed forward and cross-catalytic systems is the initial leakage, but not from the single-stranded tails of substrates in upstream layers. Therefore, if rigorous purifications of substrates were performed to reduce the initial leakage, the sensitivity of those systems is expected to significantly improve. The reason why R + S1cr + S2cr (Figure S13B) showed a higher fluorescence intensity than R + S1 + S2 (Figure S13A) is the higher background of R + S1cr than R + S1. This could be due to the single-stranded domain g2 next to domain d1s of S1cr (Figure S12A). This domain will reduce the steric hindrance for domain d1s to be hybridized with R, compared with S1 in which double-stranded domain b exists next to domain d1s (Figure S10).

Although we observed the reaction caused by cooperative binding of two single-stranded DNA strands (Figure S4D, E), the reaction uses a long toehold (10 nt). Therefore, output tails of substrates with 6 or 8 nt toehold length are less likely to cause the reaction in the same mechanism. Also, even if such reactions become significant once the initial leakage is eliminated, it will be possible to minimize such reactions using clamps.[18]

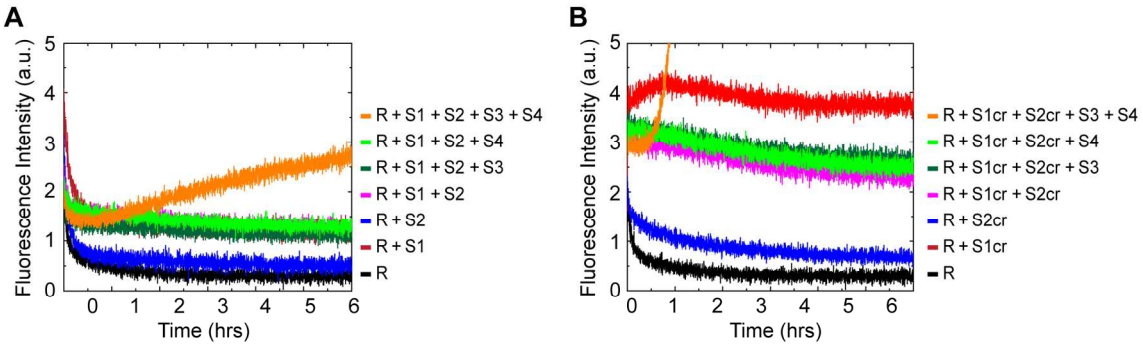

Figure S13. Background analysis of the reaction networks with the three-arm junction substrates.

For all the data, fluorescence intensity was not normalized. **(A)** Two-layer feed forward catalytic system. [S1] = [S2] = [S3] = [S4] = 50 nM, [R] = 100 nM. **(B)** Cross-catalytic system. [Scr1] = [S2cr] = [S3] = [S4] = 50 nM, [R] = 100 nM.

S9. Feed forward and autocatalytic system with three-arm junction substrates based on 16 nt specificity domains

In addition to the 22 nt specificity domains, three-arm junctions with 16 nt specificity domains were used to construct a feed forward catalytic system (Figure S14A). The leakage (0 pM) was significantly larger than that of the 22 nt design (Figure S14B), which decreased the signal to noise ratio. Considering the similar leakage rate constants for the 16 nt and 22 nt specificity domain designs (Figure S4C, S8D), we expect that the initial leakage of the 16nt design could be higher than the 22 nt design, resulting in the larger leakage of the feed forward system. An autocatalytic network was also constructed (Figure S14C), and the kinetic trace of the system again showed large leakage (Figure S14D). Moreover, the kinetic trace does not appear to have the ideal sigmoid shape. This can be seen because the 0 pM reaction slows down after 2 hours, comparing with the autocatalytic system with four-arm junction substrates (Figure 4B). The slow-down of the three-arm junction substrate is attributed to a sequence constraint, which caused one strand (light blue strand, *mB3au*) of mS2au to have a hairpin structure, destabilizing mS2au and mP3au.

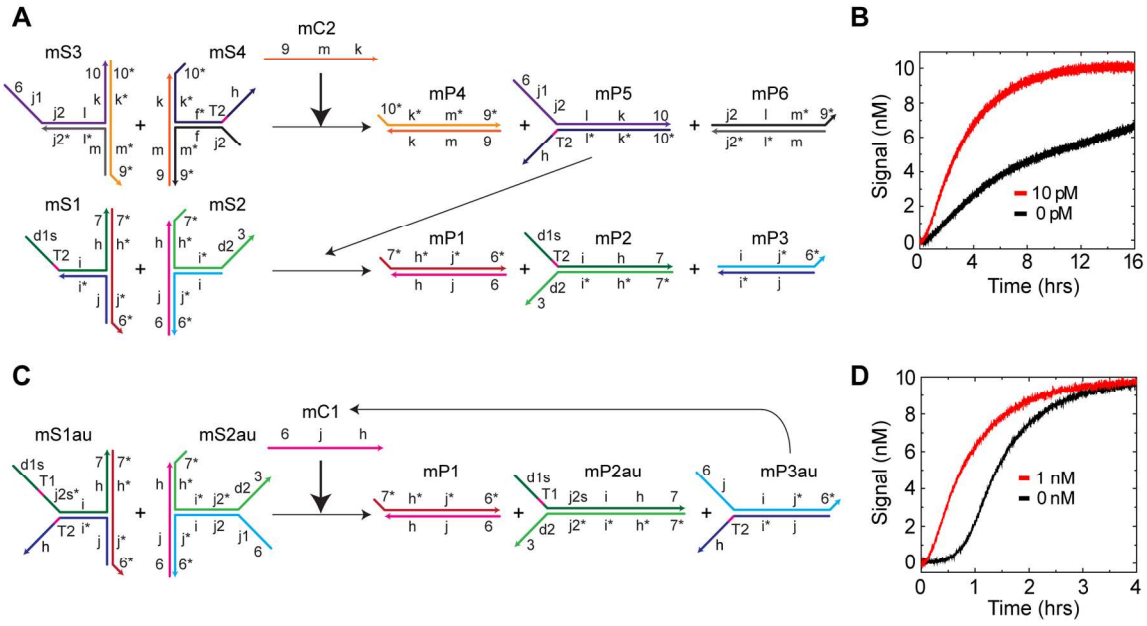

Figure S14. Three-arm junction catalytic networks based on 16 nt specific domains. (A) A simplified schematic of the two-layer feed forward catalytic system. Product mP5 has catalytic domains to act as an input catalyst for the second layer. **(B)** Kinetic traces of the feed forward catalytic system with different concentrations of the catalyst mC2. [mS1] = [mS2] = [mS3] = [mS4] = 10 nM, and [R] = 20 nM. **(C)** A

simplified schematic of the autocatalytic system. The product mP3au has the catalytic domains to cause exponential amplification. Note that the light blue strand of the substrate mS2au has domains 6-j-i-j*-6* (domain j = j1 + j2), resulting in a hairpin structure. mP2au has the output domain for the reporting reaction as mP2 (Figure S8B). Domain T1 of mS1au represents 1 nt thymidine. Domain j2s is j2 with 1 nt at 5' end deleted. **(D)** Kinetic traces of the autocatalytic network with different concentrations of the catalyst mC1. [mS1au] = [mS2au] = 10 nM, and [R] = 20 nM.

S10. Design principle of a four-arm junction substrate

The design principle of a four-arm junction substrate is identical to a three-arm junction substrate, and the IELs or each reaction is similar. However, the primary difference between them is the existence of an intermediate complex with a six-arm junction, which is shown in the following section.

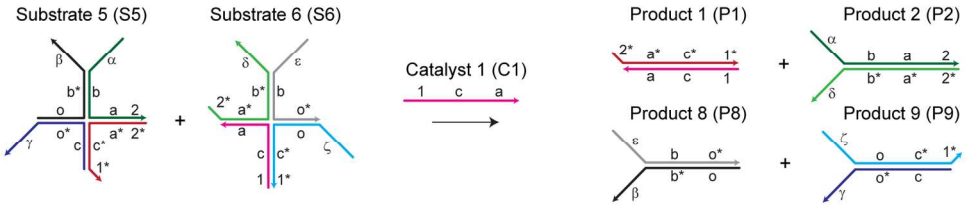

Figure S15. Design principles of a four-arm junction substrate for a catalytic system. The reaction converts two substrates S5 and S6 into four products P1, P2, P8, and P9. Products P2, P8 and P9 have a new combination of output domains α and δ, ε and β, ζ and γ, respectively. Sequences of those output are independent of the catalyst C1, therefore can be used for signal cascades.

S11. Toehold length variations of four-arm junction substrates

Here, a single-layer catalytic system was used in order to test the operation of four-arm junction substrates (Figure S16A), and the initial design with a 6 nt toehold showed a very slow catalytic reaction (Figure S16B). Therefore, the toehold length was changed systematically from 6 nt to 8 nt. As a result, the reaction between the intermediate I5 and S6 was found to be the rate limiting step, because the overall catalytic reaction sped up only when domain 2 was extended, which acted as the toehold to drive the reaction between I5 and S6 (Figure S16C-E). This performance change is because of the high energy barrier imposed by the six-arm junction structure[15] on I6 (Figure S16A). For the above listed substrates, toeholds were extended unevenly so that toehold hybridization occurred via 8 nt, but dissociation occurred via 6 nt in order to maintain fast dissociation. In fact, the catalytic turnover became lower if both the hybridization and dissociation of the toehold occurred with a 8 nt toehold (Figure S16F). The process of toehold dissociation becomes more challenging for longer toeholds, which will be required for five-arm junction substrates because eight-arm junctions will emerge during the catalytic reaction (Figure

S21). In addition to domain 2, the extended domain 1 allowed the output catalyst to trigger the catalytic reaction as quick as the single-stranded catalyst (Figure S9G, H), which is the reason why substrates S5xy and S6xy were adapted for the autocatalytic system in Figure 4.

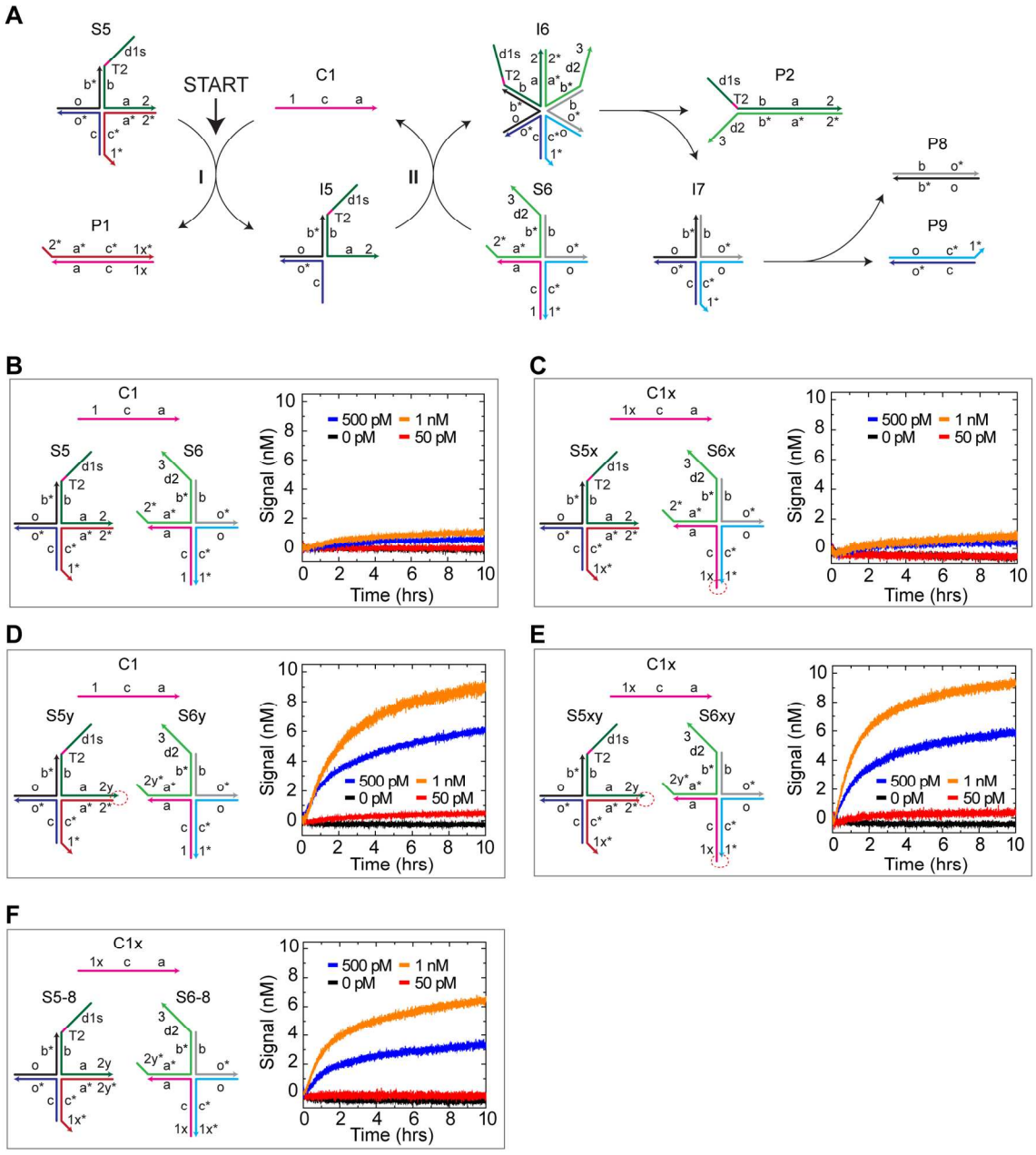

Figure S16. Variations of toehold designs for four-arm junction substrates. (A) A schematic of the catalytic pathway for the single-layer catalytic network. **(B)-(F)** Kinetic traces with different catalytic concentrations. [S5] = [S6] = 10 nM, [R] = 20 nM, and those were the same concentrations for all other variations. 2 nt were added at 5' end of domain 1 and 3' end of domain 2 (both are 6 nt) to generate

domains 1x and 2y (both are 8 nt), respectively. The toehold affects the kinetics of step **I** (the reaction between the substrate S5 and the catalyst C1), and step **II** (the reaction between the intermediate I5 and the substrate S6). Red dot circles show the exposed 2 nt toeholds. **(B)** 6 nt design for both toehold domains 1 and 2. **(C)** The toehold domain 1 was unevenly extended on the substrate S6x. As a result, step **I** occurs via 8 nt toehold hybridization and 6 nt toehold dissociation, while step **II** occurs via 6 nt toehold hybridization and 6 nt toehold dissociation. **(D)** The toehold domain 2 was unevenly extended on the substrate S5y. As a result, step **I** occurs via 6 nt toehold hybridization and 6 nt toehold dissociation, while step **II** occurs via 8 nt toehold hybridization and 6 nt toehold dissociation. **(E)** Both toehold domains 1 and 2 were unevenly extended so that both steps **I** and **II** occur via 8 nt toehold hybridization and 6 nt toehold dissociation. **(F)** Both toehold domain 1 and 2 were evenly extended so that both steps **I** and **II** occur via 8 nt toehold hybridization and 8 nt toehold dissociation.

S12. Calculation of rate constants and kinetic simulation for four-arm junction substrates

The catalytic rate constant and leakage rate constant – The catalytic rate constant for four-arm junction substrates, with extended toeholds at domains 1 and 2, were calculated. Using the same process outlined in Section S3, we obtained $k_{cat} = 2.28 \cdot 10^{13}$ $M^{-2}s^{-1}$ from the 1 nM catalytic reaction (Figure S17A), which is almost identical to the three-arm junction substrates (Table 1). We did not use the 500 pM catalytic reaction because the reaction nearly stalled at 10 hours (Figure S16E). The leakage reactions were also performed for four-arm junction substrates with their corresponding background reactions (Figure S17B). Then, after using the same process in Section S3, the leakage rate constants were calculated from 20 to 24 hours (Figure S17C, D). The values were $k_{leak2} = 2.11 \cdot 10^{-2}$ $M^{-1}s^{-1}$ for S5xy + S6xy and $k_{leak} = 2.66 \cdot 10^{-2}$ $M^{-1}s^{-1}$ for S5 + S6. While there is no significant difference on the rate constants between the two designs, the S5xy and S6xy have two sets of exposed 2 nt toehold (Figure S16E), which can hybridize to each other and initiate strand displacement. This result is in agreement with a prior toehold mediated, four-way branch migration study,[10] which reported the same kinetic rate constants between a zero toehold and an "open" 2 nt toehold. However, since the background signal caused by the single-stranded tail on the substrates might exist (Figure S4D, E), we cannot exclude the possibility that the actual leakage rates of the two designs are significantly different.

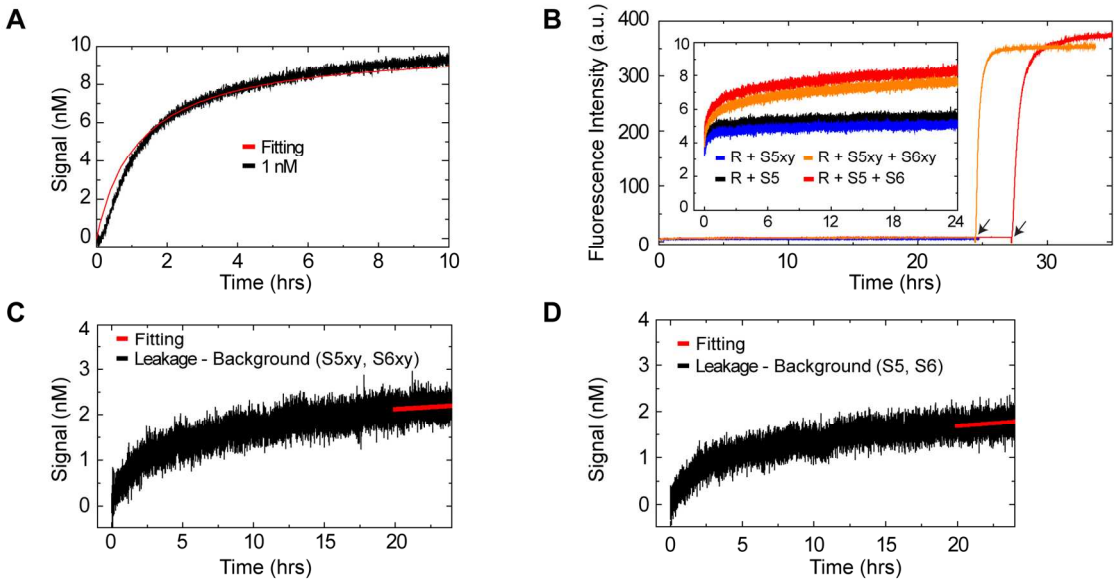

Figure S17. The rate constants calculation of single-layer catalytic system with four-arm junction substrates. (A) The kinetic trace of the four-arm junction substrates with 1 nM catalyst C1x was fit to equation (6), and k_{cat} = 2.28 · 10^{13} $M^{-2}s^{-1}$ was extracted. [S5xy] = [S6xy] = 10 nM, [R] = 20 nM. **(B)** Kinetic traces of leakages and the background reactions for the four-arm junction substrates. [S5xy] = [S6xy] = [S5] = [S6] = 500 nM, [R] = 700 nM. Leakage traces are R + S5xy + S6xy and R + S5 + S6, and other traces are performed to measure the background signals. Fluorescence data is not normalized. Black arrows show the addition of catalyst C1. **(C)** The background reaction (R + S5xy) was subtracted from the leakage (R + S5xy + S6xy), and the initial fluorescence intensity was adjusted to zero. Then, the fluorescence intensity was normalized using the average of maximum fluorescence changes of 10 nM concentration experiments in Figure S16E. Finally, the initial slope (20 to 24 hours) was fit to equation (8), and k_{leak2} = 2.11 · 10^{-2} $M^{-1}s^{-1}$ was extracted. **(D)** The background reaction (R + S5) was subtracted from the leakage reaction (R + S5 + S6), and the initial fluorescence intensity was adjusted to zero. Then, the fluorescence intensity was normalized using the average maximum fluorescence changes of the 10 nM concentration experiments in Figure S16B. Finally, the initial slope (20 to 24 hours) was fit to equation (8), and k_{leak} = 2.66 · 10^{-2} $M^{-1}s^{-1}$ was extracted.

Kinetic simulation – Based on Figure S16A and E, the following equations can be made for substrates S5xy and S6xy.

$$\mathrm{S5xy} + \mathrm{S6xy} \xrightarrow{k_{leak2}} \mathrm{P1} + \mathrm{P2} + \mathrm{P8} + \mathrm{P9} \tag{36}$$

$$\mathrm{C1x} + \mathrm{S5xy} \underset{k_{-1}}{\overset{k_1}{\rightleftharpoons}} \mathrm{P1} + \mathrm{I5} \tag{37}$$

$$\mathrm{I5} + \mathrm{S6xy} \underset{k_{-2}}{\overset{k_2}{\rightleftharpoons}} \mathrm{I6} + \mathrm{C1x} \tag{38}$$

$$\mathrm{I6} \xrightarrow{k_3} \mathrm{P2} + \mathrm{P8} + \mathrm{P9} \quad (39)$$

$$\mathrm{P2} + \mathrm{R} \xrightarrow{k_4} \mathrm{Rw} + \mathrm{D} \quad (40)$$

$$\mathrm{C1x} + \mathrm{S5xyd} \xrightarrow{k_1} \mathrm{P1} + \mathrm{I5d} \quad (41)$$

$$\mathrm{I5} + \mathrm{S6xyd} \xrightarrow{k_2} \mathrm{I6} + \mathrm{C1xd} \quad (42)$$

$$\mathrm{S5xyi} + \mathrm{S6xyi} \xrightarrow{k_i} \mathrm{P1} + \mathrm{P2} + \mathrm{P8} + \mathrm{P9} \quad (43)$$

Production of P8 and P9 from intermediate I7 was included into equation (39) for simplification. Other than the leakage rate constant (k_{leak2} = 2.11 · 10^{-2} $M^{-1}s^{-1}$) we used the same rate constants for the three-arm junction substrates in Figure S7. The population of defect-substrates S5xyd and S6xyd were adjusted to be 4 %, and the initial leakage substrates S5xyi and S6xyi were adjusted to be 0.4 %. The simulation result using equations (36) through (43) is shown in Figure S18.

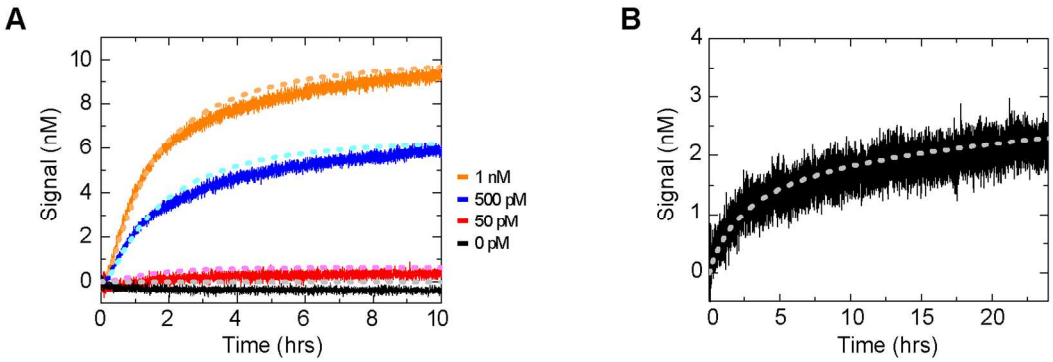

Figure S18. Kinetic simulation for single-layer catalytic system with four-arm junction substrate. (A) 10 nM concentration of substrates with different concentration of catalyst for the data in Figure S16E. Kinetic simulations are shown as dots with weak colors. **(B)** Leakage reaction at 500 nM concentration of substrates for the data in Figure S17C.

S13. Detailed reaction schematic and kinetic simulation of autocatalytic system with four-arm junction substrates

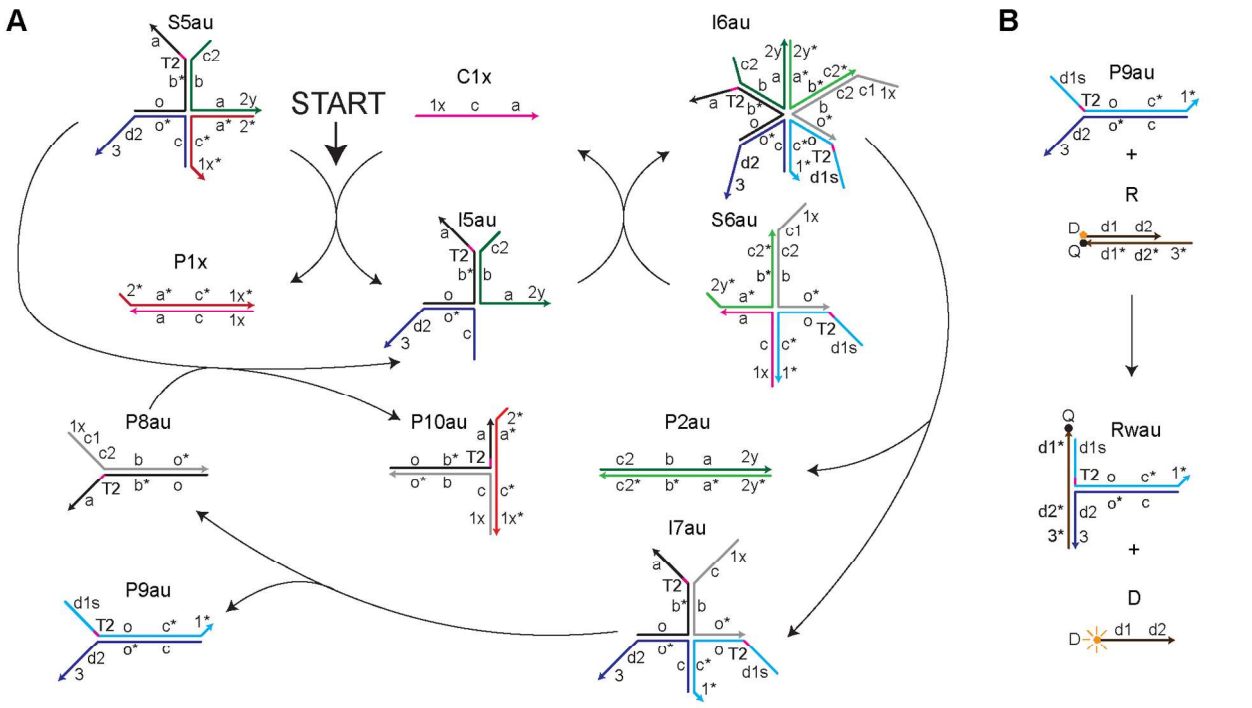

Figure S19. The detailed reaction schematic of the autocatalytic system with four-arm junction substrates. (A) A schematic of the catalytic pathway. The pathway starts with the reaction between the substrate S5au and the catalyst C1x. The single-stranded sequence of the product P8au has the same domain as the catalyst C1x. Domain c = domains c1 + c2. **(B)** The reporting reaction. The reporter complex R is the same as all other experiments.

Based on Figure S19A and B, the following equations can be made for the autocatalytic system.

$$\mathrm{S5au} + \mathrm{S6au} \xrightarrow{k_{leak2}} \mathrm{P1x} + \mathrm{P2au} + \mathrm{P8au} + \mathrm{P9au} \tag{44}$$

$$\mathrm{C1x} + \mathrm{S5au} \underset{k_{-1}}{\overset{k_1}{\rightleftharpoons}} \mathrm{P1x} + \mathrm{I5au} \tag{45}$$

$$\mathrm{I5au} + \mathrm{S6au} \underset{k_{-2}}{\overset{k_2}{\rightleftharpoons}} \mathrm{I6au} + \mathrm{C1x} \tag{46}$$

$$\mathrm{I6au} \xrightarrow{k_3} \mathrm{P2au} + \mathrm{P8au} + \mathrm{P9au} \tag{47}$$

$$\mathrm{P8au} + \mathrm{S5au} \underset{k_{-10}}{\overset{k_{10}}{\rightleftharpoons}} \mathrm{P10au} + \mathrm{I5au} \tag{48}$$

$$\mathrm{P9au} + \mathrm{R} \xrightarrow{k_4} \mathrm{Rwau} + \mathrm{D} \tag{49}$$

$$\mathrm{C1x} + \mathrm{S5aud} \xrightarrow{k_1} \mathrm{P1x} + \mathrm{I5aud} \tag{50}$$

$$\mathrm{P8au} + \mathrm{S5aud} \xrightarrow{k_{10}} \mathrm{P10au} + \mathrm{I5aud} \tag{51}$$

$$\mathrm{I5au} + \mathrm{S6aud} \xrightarrow{k_2} \mathrm{I6au} + \mathrm{C1xd} \tag{52}$$

$$\mathrm{S5aui} + \mathrm{S6aui} \xrightarrow{k_i} \mathrm{P1x} + \mathrm{P2au} + \mathrm{P8au} + \mathrm{P9au} \quad (53)$$

The overall speed of the single-layer catalytic reaction was shown to be approximately the same when the output catalyst P8au was used instead of C1x (Figure S9H). This trend holds true even if the reaction rate used in equation (48), with P8au catalyst, is a few times slower than the reaction rate used in equation (45), with the single-stranded catalyst C1x. This trend is because P8au is consumed by S5xy and a new catalyst, C1x, is generated, which causes an initial delay of the overall catalytic reaction that is quickly recovered by releasing C1x from substrate S6xy. Therefore, we used $k_{10} = k_{-10} = k_1/2.5$ and the experimental data was simulated well (Figure S20A). The simulation result using equations (44) through (53) for the autocatalytic system is shown in Figure S20B. Here, the population of defect-substrates and initial leakage substrates were assumed to be the same as the single-layer catalytic system so that S5aud and S6aud had a 4 % defect rate, while S5aui and S6aui had a 0.4 % defect rate. The initial concentration of P8au was adjusted to be 1.5 pM. The agreement of the data and the simulation is better than the two-layer feed forward (Figure S11B) and the cross-catalytic system (Figure S12C) because the P8au catalyst (Figure S20A) is well-simulated when compared to the P5 catalyst (Figure S11A).

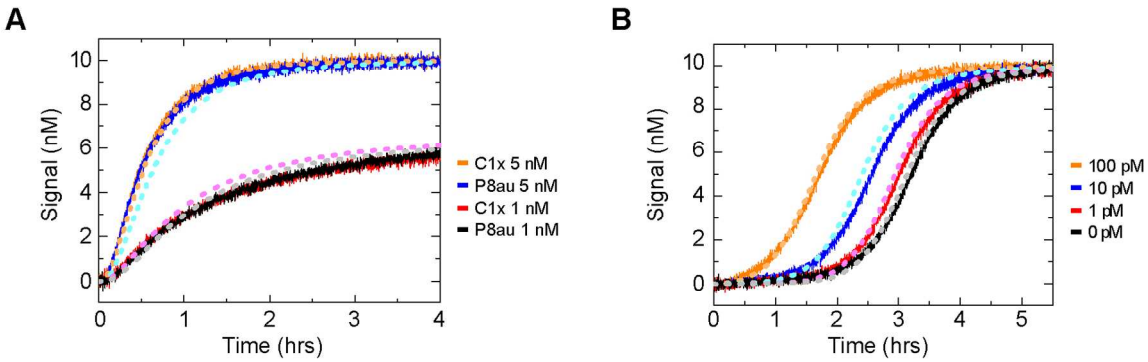

Figure S20. Kinetic simulation for autocatalytic system with four-arm junction substrate. (A) Simulation for data in Figure S9H, where single-stranded catalyst C1x and junction catalyst P8au were used as input catalyst for single-layer catalytic system with substrate S5xy and S6xy. Since unpurified DNA strands were used for this set of experiment, the population of defect-substrates S5xyd and S6xyd were adjusted to be 8 %. **(B)** Simulation for the autocatalytic system in Figure 4B.

S14. Proposed design of a five-arm junction substrate

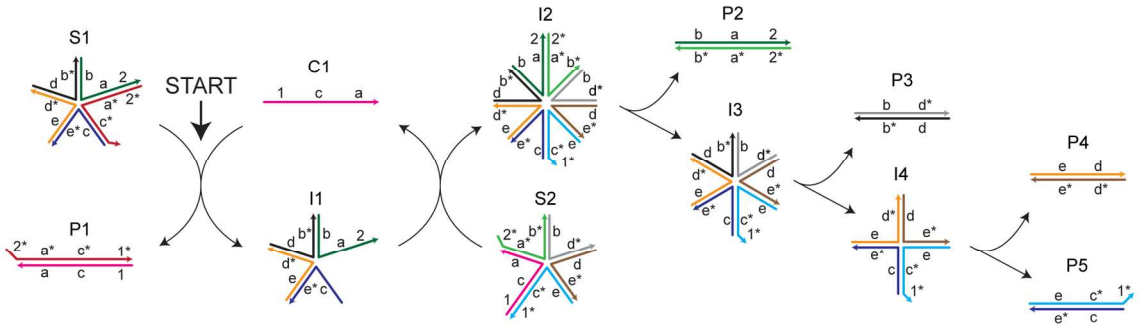

Figure S21. Single-layer catalytic system with five-arm junction substrates. A proposed design and a schematic of the catalytic pathway. Naming of domains, a catalyst, and other DNA complexes are unrelated to those in other schematics. For simplicity, single-stranded tails on each substrate, which can be used for the formation of output signals, are not shown.

S15. Gel images

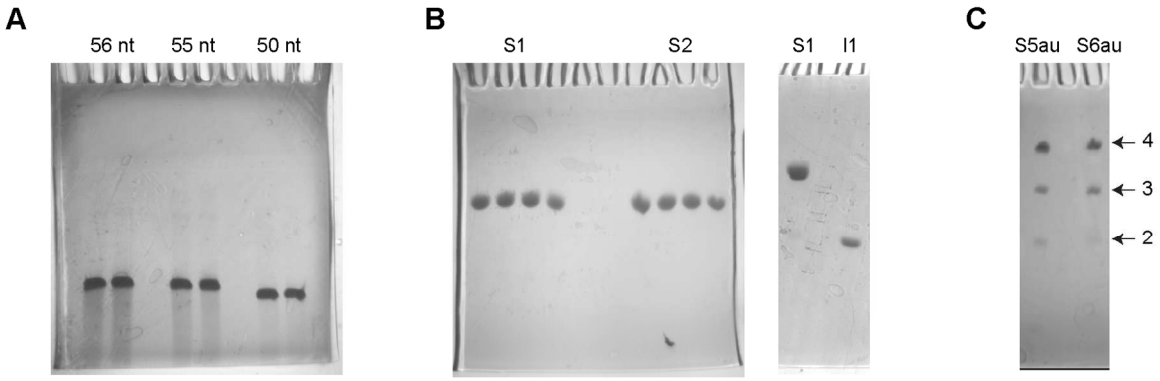

Figure S22. Relative mobility of single-stranded DNAs and DNA complexes. (A) A 10 % denature PAGE for unpurified DNA strands purchased from IDT. The first two lanes are the *tC1* strands with 56 nt, the middle two lanes are the *tC3* strands with 55 nt, and the last two lanes are the *tD1* strands with 50 nt. All sequences are shown in Table S1. Denature PAGE was performed to remove smear bands from the target strands. Since the separation of 56 nt and 55 nt was very small for our experimental condition, we do not expect purification of full length DNA strands from the n-1 truncated strands that are common during chemical DNA synthesis.[23] **(B)** 10 % native PAGE. The gel image on the left side shows the purification process of DNA complex S1 and S2, where an equal stoichiometric ratio was used for the complex formation. The running time of the gel was 5 hours. The small gel image on the right side shows the relative mobility of S1, with strands *A1*, *A2*, and *A3*, and intermediate I1, with strands *A2* and *A3*. The running time of the gel was 4 hours. The separation of S1 and I1 are large enough for easy purification at

4 hours. Therefore, even if I1 is formed during the formation of S1, due to concentration error, S1 can be purified under our experimental conditions. **(C)** 10 % native PAGE for the purification process of DNA complex S5au and S6au. Those complexes were annealed with uneven stoichiometric ratios, as explained in the experimental methods in Section S16. Consequently, three bands appeared on each lane, which included a: (a) four-stranded complex, (b) three-stranded complex, and (c) small amount of two-stranded complex. The number of stands in the gel is labeled and decreases from top to bottom. However, the band separations were large enough so that the target four-stranded DNA complexes could be purified.

S16. Experimental methods

Unless otherwise specified, all of the chemicals were purchased from Thermo Fisher Scientific.

Formation of multi-arm junction substrates – DNA strands were purchased from Integrated DNA Technologies (IDT) and re-suspended to be 100 μM in 1×TE buffer (10 mM Tris–HCl, pH 8.0, 1 mM EDTA), diluted from 100×TE (Sigma-Aldrich). The *d* strand was modified with 5' Tetrachlorofluorescein (TET) and the *q* strand was modified with 3' Iowa black dark quenchers (IABkFQ), both of which were purchased with HPLC purification. All other strands were purchased as unpurified, then purified by denature polyacrylamide gel electrophoresis (denature PAGE) in house, otherwise mentioned. For substrate formation, each DNA strand was stoichiometry mixed in 1×TE buffer with 12.5 mM $MgCl_2$ (1×TE/Mg^{2+}). However, a non-stoichiometry concentration was used for the following substrates: (1) S5au (with *A1x* strand 50% shortage), S6au (with *fB4au* strand 50% shortage), and mS1au (with *mA1* strand 30 % shortage), because the excess of those strands can hybridize to the ssDNA tails on the substrates, and might not be separated even after native PAGE purification; (2) mS2 (with *mB3* strand 30% shortage), because the *mB3* strand hybridized with the ssDNA tail on the mS2 substrate due to unintentional complementarity; (3) S4 (with *tD1* strand 50 % excess), because stoichiometry formation showed a small complex population of *tD2-tD3*. This could be due to the inaccuracy of the concentration of either strand; (4) S2 (with *B1* strand 50% excess) only in Figure 3B, because it showed a better catalytic turnover than the stoichiometric formation. Annealing of DNA complexes was performed at 90 °C for 5 minutes and cooled to 20 °C at a rate of 0.1 °C per 10 seconds. This slow annealing rate was necessary to form the mS2au substrate because of the hairpin structure on the *mB3au* strand, but not necessary for the other substrates.

Gel electrophoresis – The gel size used in all the experiments was 1.5 mm thick 10 × 10 cm.

For denature PAGE, 10% gel (acrylamide:bis = 29:1 from Bio-Rad) was made with 1×TBE buffer (89 mM Tris, 89 mM boric acid, 2 mM EDTA) and 8 M Urea (ultrapure) from MP Biomedicals. Then, ~15 μL of 100 μM DNA was mixed with equal volume to the loading buffer, which was 8:1:1 volume ratio mixture of formamide (Sigma-Aldrich), bromophenol blue (Sigma-Aldrich), and 10×TBE. Next, the DNA solution was loaded in each lane and run at ~400V for 30 to 40 minutes with

circulating water at 60 °C. The bands of interest were cut out, crushed by pipet tips, and eluted in 300 μL of 1×TE buffer overnight. After gel fragments were removed via a centrifuge, 3 M of sodium acetate (Arbor Scientific) (pH 5.2) was added to a final concentration of 0.3 M. Then, 1 mL of 100% Ethanol were added. After cooling at -20 °C for ~1 hour, centrifugation was performed with 15,000 rcf at 4 °C for 20 minutes. The DNA pellet was further rinsed by adding 1 mL of 70% Ethanol, and centrifuged at 15,000 rcf at 4 °C for 20 minutes. Finally, the ethanol solution was removed and the remaining solution was air dried for ~30 minutes, and 30 μL of 1×TE was added.

For native PAGE, 10% gel (acrylamide:bis = 29:1) was made with 1×TAE buffer (40 mM Tris, 40 mM Acetate, 1 mM EDTA) and supplemented with 12.5 mM $Mg(C_2H_3O_2)_2$. Then, DNA complexes were mixed with 1/4 volume of loading buffer, which was 1:1 volume ratio mixture of bromophenol blue dye (Sigma-Aldrich) and a ficoll solution (type 400, 20 % water from Sigma-Aldrich). Next, the DNA complex solution was loaded and run at 150V for ~5 hours with circulating water at 20 °C. The bands of interest were then cut out of the gels, not crushed, and eluted in 1×TE/Mg^{2+} for 2 days at 4 °C. For Figure S9D, the gel was stained with SYBR Gold for 30 minutes.

In all the cases, DNA concentrations were quantified by absorbance at 260 nm and calculated using extinction coefficients provided by IDT for single-stranded and double-stranded DNA.[24]

Kinetics experiments – All kinetic experiments were performed at 25 °C in 1×TE/Mg^{2+} using two fluorescence spectrophotometers (Agilent Technologies, Cary Eclipse) at 521 nm excitation and 538 nm emission with 0.56 mL Special Optical Glass cuvettes (Starna Cells). To prevent solution evaporation, the lid was covered with parafilm. Slit sizes were 2.5 nm for the excitation and 10 nm for the emission. A poly-T solution (dT_{20} or dT_{50}, both did not show any difference) were added to all dilute stock samples (1 μM and lower) with 1 μM in order to minimize the loss of DNA via sticking to the sample tubes and pipet tips.[1] Fluorescence data was then normalized so that the initial fluorescence intensity corresponds to 0 nM and the final intensity corresponded to the initial concentration of the substrates (under the assumption that all substrates were consumed), otherwise mentioned. When the reaction did not reach completion during the experimental time windows, high concentration of catalysts was added to drive the reaction to completion. For the two cases with the four-arm junction substrates (S5 + S6 and S5x + S6x), their maximum intensity was obtained by heating up the sample cuvette in hot water, because of their slow catalytic rates. For fluoresce data where an intensity was not normalized, all kinetic traces were acquired by using the same machine, except the data in Figure S13A. In this data, R + S1 and R + S2 were performed by using a different machine from the other kinetic traces. Therefore, typical fluorescence intensity difference, 5%, was used to correct the intensity for R + S1 and R + S2.

S17. DNA strand sequences

The domains and sequences of DNA strands used for each DNA complex are shown in Table S1. DNA sequences were designed by NUPACK[20] or EGNAS,[25] then occasionally modified by hand to minimize the secondary structure and hybridization of unrelated domains.

Table S1. Strand sequences for DNA complexes used.

Complex	Name	domains	Sequence (5` to 3`)
S1	*A1*	2*-a*-c*-1*	GGATGT GCTAGGTGGTGACTTGGGACTG GAACGAATGGCTGCTGATCTGG AAACGG
	A2	d1s-T2-b-a-2	CCAAACCTTCATCTTC TT GCACTCGCGATACGAGGCCTGG CAGTCCCAAGTCACCACCTAGC ACATCC
	A3	c-b*	CCAGATCAGCAGCCATTCGTTC CCAGGCCTCGTATCGCGAGTGC
S2	*B1*	1-c-a	CCGTTT CCAGATCAGCAGCCATTCGTTC CAGTCCCAAGTCACCACCTAGC
	B2	2*-a*-b*-d2-3	GGATGT GCTAGGTGGTGACTTGGGACTG CCAGGCCTCGTATCGCGAGTGC TACTCG CCTCTACTCA
	B3	b-c*-1*	GCACTCGCGATACGAGGCCTGG GAACGAATGGCTGCTGATCTGG AAACGG
S3	*tC1*	5*-e*-g*-4*	GGTGTT CGGGAGTAGGGTAGAGTAAGAG GAAGGTAGAGCGGAGTAACAGG GATAGC
	tC2	1-c1-c2-f-e-5	CCGTTT CCAGATCAGCA GCCATTCGTTC GCGAGTGTCCTGGGTCAAGGCG CTCTTACTCTACCCTACTCCCG AACACC
	tC3	g-f*-c2*	CCTGTTACTCCGCTCTACCTTC CGCCTTGACCCAGGACACTCGC GAACGAATGGC
S4	*tD1*	4-g-e	GCTATC CCTGTTACTCCGCTCTACCTTC CTCTTACTCTACCCTACTCCCG
	tD2	5*-e*-f*-T2-a	GGTGTT CGGGAGTAGGGTAGAGTAAGAG CGCCTTGACCCAGGACACTCGC TT CAGTCCCAAGTCACCACCTAGC
	tD3	c2-f-g*-4*	GCCATTCGTTC GCGAGTGTCCTGGGTCAAGGCG GAAGGTAGAGCGGAGTAACAGG GATAGC
S1cr	*A1*	2*-a*-c*-1*	GGATGT GCTAGGTGGTGACTTGGGACTG GAACGAATGGCTGCTGATCTGG AAACGG
	A2cr	d1s-T2-g2-b-a-2	CCAAACCTTCATCTTC TT GCTCTACCTTC GCACTCGCGATACGAGGCCTGG CAGTCCCAAGTCACCACCTAGC ACATCC
	A3cr	c-b*-T2-e	CCAGATCAGCAGCCATTCGTTC CCAGGCCTCGTATCGCGAGTGC TT CTCTTACTCTACCCTACTCCCG
S2cr	*B1*	1-c-a	CCGTTT CCAGATCAGCAGCCATTCGTTC CAGTCCCAAGTCACCACCTAGC
	B2cr	2*-a*-b*-g2*-d2-3	GGATGT GCTAGGTGGTGACTTGGGACTG CCAGGCCTCGTATCGCGAGTGC GAAGGTAGAGC TACTCG CCTCTACTCA
	B3cr	4-g1-g2-b-c*-1*	GCTATC CCTGTTACTCC GCTCTACCTTC GCACTCGCGATACGAGGCCTGG GAACGAATGGCTGCTGATCTGG AAACGG
mS1	*mA1*	7*-h*-j*-6*	GGTGTC GGCGGTGTTGTTAGTG GAATGCGGAGGAGTGG AAACGG
	mA2	d1s-T2-i-h-7	CCAAACCTTCATCTTC TT GCGATGTGGTGAGAGG CACTAACAACACCGCC GACACC
	mA3	j-i*	CCACTCCTCCGCATTC CCTCTCACCACATCGC
mS2	*mB1*	6-j-h	CCGTTT CCACTCCTCCGCATTC CACTAACAACACCGCC
	mB2	7*-h*-i*-d2-3	GGTGTC GGCGGTGTTGTTAGTG CCTCTCACCACATCGC TACTCG CCTCTACTCA
	mB3	i-j*-6*	GCGATGTGGTGAGAGG GAATGCGGAGGAGTGG AAACGG
mS3	*mC1*	10*-k*-m*-9*	GCTTGT GGAGATTTAGGCGTTG GTTCAGGTAGGTTCGG AATAGC
	mC2	6-j1-j2-l-k-10	CCGTTT CCACTCCTCCGCATTC GGTTATGGCTGGTTTC CAACGCCTAAATCTCC ACAAGC
	mC3	m-l*-j2*	CCGAACCTACCTGAAC GAAACCAGCCATAACC GAATGC
mS3u	*mC1*	10*-k*-m*-9*	GCTTGT GGAGATTTAGGCGTTG GTTCAGGTAGGTTCGG AATAGC
	mC2	6-j1-j2-l-k-10	CCGTTT CCACTCCTCC GCATTC GGTTATGGCTGGTTTC CAACGCCTAAATCTCC ACAAGC
	mC3u	m-l*	CCGAACCTACCTGAAC GAAACCAGCCATAACC
mS4	*mD1*	9-m-k	GCTATT CCGAACCTACCTGAAC CAACGCCTAAATCTCC

	mD2	10*-k*-l*-2T-h	GCTTGT GGAGATTTAGGCGTTG GAAACCAGCCATAACC TT CACTAACAACACCGCC
	mD3	j2-l-m*-9*	GCATTC GGTTATGGCTGGTTTC GTTCAGGTAGGTTCGG AATAGC
mP5	*mC2*	6-j1-j2-l-k-10	CCGTTT CCACTCCTCCGCATTC GGTTATGGCTGGTTTC CAACGCCTAAATCTCC ACAAGC
	mD2	10*-k*-l*-2T-h	GCTTGT GGAGATTTAGGCGTTG GAAACCAGCCATAACC TT CACTAACAACACCGCC
mP5-t	*mC2*	6-j1-j2-l-k-10	CCGTTT CCACTCCTCCGCATTC GGTTATGGCTGGTTTC CAACGCCTAAATCTCC ACAAGC
	mD2-T	10*-k*-l*-h	GCTTGT GGAGATTTAGGCGTTG GAAACCAGCCATAACC CACTAACAACACCGCC
mP5s	*mC2s*	6-j1-l-k-10	CCGTTT CCACTCCTCC GGTTATGGCTGGTTTC CAACGCCTAAATCTCC ACAAGC
	mD2s	10*-k*-l*-2T j2-h	GCTTGT GGAGATTTAGGCGTTG GAAACCAGCCATAACC TT GCATTC CACTAACAACACCGCC
mP5-t	*mC2s*	6-j1-l-k-10	CCGTTT CCACTCCTCC GGTTATGGCTGGTTTC CAACGCCTAAATCTCC ACAAGC
	mD2s-T	10*-k*-l*-j2-h	GCTTGT GGAGATTTAGGCGTTG GAAACCAGCCATAACC GCATTC CACTAACAACACCGCC
mS1au	*mA1*	7*-h*-j*-6*	GGTGTC GGCGGTGTTGTTAGTG GAATGCGGAGGAGTGG AAACGG
	mA2au	d1s-T1-j2s-i-h-7	CCAAACCTTCATCTTC T CATTC GCGATGTGGTGAGAGG CACTAACAACACCGCC GACACC
	mA3au	j-i*-T2-h	CCACTCCTCCGCATTC CCTCTCACCACATCGC TT CACTAACAACACCGCC
mS2au	*mB1*	6-j-h	CCGTTT CCACTCCTCCGCATTC CACTAACAACACCGCC
	mB2au	7*-h*-i*-j2*-d2-3	GGTGTC GGCGGTGTTGTTAGTG CCTCTCACCACATCGC GAATGC TACTCG CCTCTACTCA
	mB3au	6-j1-j2-i-j*-6*	CCGTTT CCACTCCTCC GCATTC GCGATGTGGTGAGAGG GAATGCGGAGGAGTGG AAACGG
S5	*A1*	2*-a*-c*-1*	GGATGT GCTAGGTGGTGACTTGGGACTG GAACGAATGGCTGCTGATCTGG AAACGG
	A2	d1s-T2-b-a-2	CCAAACCTTCATCTTC TT GCACTCGCGATACGAGGCCTGG CAGTCCCAAGTCACCACCTAGC ACATCC
	fA3	o-b*	GGCACCTATCGACACCTCACGC CCAGGCCTCGTATCGCGAGTGC
	fA4	c-o*	CCAGATCAGCAGCCATTCGTTC GCGTGAGGTGTCGATAGGTGCC
S5x	*A1x*	2*-a*-c*-1x*	GGATGT GCTAGGTGGTGACTTGGGACTG GAACGAATGGCTGCTGATCTGG AAACGGTG
	A2	d1s-T2-b-a-2	CCAAACCTTCATCTTC TT GCACTCGCGATACGAGGCCTGG CAGTCCCAAGTCACCACCTAGC ACATCC
	fA3	o-b*	GGCACCTATCGACACCTCACGC CCAGGCCTCGTATCGCGAGTGC
	fA4	c-o*	CCAGATCAGCAGCCATTCGTTC GCGTGAGGTGTCGATAGGTGCC
S5y	*A1*	2*-a*-c*-1*	GGATGT GCTAGGTGGTGACTTGGGACTG GAACGAATGGCTGCTGATCTGG AAACGG
	A2y	d1s-T2-b-a-2y	CCAAACCTTCATCTTC TT GCACTCGCGATACGAGGCCTGG CAGTCCCAAGTCACCACCTAGC ACATCCTC
	fA3	o-b*	GGCACCTATCGACACCTCACGC CCAGGCCTCGTATCGCGAGTGC
	fA4	c-o*	CCAGATCAGCAGCCATTCGTTC GCGTGAGGTGTCGATAGGTGCC
S5xy	*A1x*	2*-a*-c*-1x*	GGATGT GCTAGGTGGTGACTTGGGACTG GAACGAATGGCTGCTGATCTGG AAACGGTG
	A2y	d1s-T2-b-a-2y	CCAAACCTTCATCTTC TT GCACTCGCGATACGAGGCCTGG CAGTCCCAAGTCACCACCTAGC ACATCCTC
	fA3	o-b*	GGCACCTATCGACACCTCACGC CCAGGCCTCGTATCGCGAGTGC
	fA4	c-o*	CCAGATCAGCAGCCATTCGTTC GCGTGAGGTGTCGATAGGTGCC
S5-8	*A1xy*	2y*-a*-c*-1x*	GAGGATGT GCTAGGTGGTGACTTGGGACTG GAACGAATGGCTGCTGATCTGG AAACGGTG
	A2y	d1s-T2-b-a-2y	CCAAACCTTCATCTTC TT GCACTCGCGATACGAGGCCTGG CAGTCCCAAGTCACCACCTAGC ACATCCTC
	fA3	o-b*	GGCACCTATCGACACCTCACGC CCAGGCCTCGTATCGCGAGTGC
	fA4	c-o*	CCAGATCAGCAGCCATTCGTTC GCGTGAGGTGTCGATAGGTGCC
S6	*B1*	1-c-a	CCGTTT CCAGATCAGCAGCCATTCGTTC CAGTCCCAAGTCACCACCTAGC
	B2	2*-a*-b*-d2-3	GGATGT GCTAGGTGGTGACTTGGGACTG CCAGGCCTCGTATCGCGAGTGC TACTCG CCTCTACTCA
	fB3	b-o*	GCACTCGCGATACGAGGCCTGG GCGTGAGGTGTCGATAGGTGCC

	fB4	o-c*-1*	GGCACCTATCGACACCTCACGC GAACGAATGGCTGCTGATCTGG AAACGG
S6x	*B1x*	1x-c-a	CACCGTTT CCAGATCAGCAGCCATTCGTTC CAGTCCCAAGTCACCACCTAGC
	B2	2*-a*-b*-d2-3	GGATGT GCTAGGTGGTGACTTGGGACTG CCAGGCCTCGTATCGCGAGTGC TACTCG CCTCTACTCA
	fB3	b-o*	GCACTCGCGATACGAGGCCTGG GCGTGAGGTGTCGATAGGTGCC
	fB4	o-c*-1*	GGCACCTATCGACACCTCACGC GAACGAATGGCTGCTGATCTGG AAACGG
S6y	*B1*	1-c-a	CCGTTT CCAGATCAGCAGCCATTCGTTC CAGTCCCAAGTCACCACCTAGC
	B2y	2y*-a*-b*-d2-3	GAGGATGT GCTAGGTGGTGACTTGGGACTG CCAGGCCTCGTATCGCGAGTGC TACTCG CCTCTACTCA
	fB3	b-o*	GCACTCGCGATACGAGGCCTGG GCGTGAGGTGTCGATAGGTGCC
	fB4	o-c*-1*	GGCACCTATCGACACCTCACGC GAACGAATGGCTGCTGATCTGG AAACGG
S6xy	*B1x*	1x-c-a	CACCGTTT CCAGATCAGCAGCCATTCGTTC CAGTCCCAAGTCACCACCTAGC
	B2y	2y*-a*-b*-d2-3	GAGGATGT GCTAGGTGGTGACTTGGGACTG CCAGGCCTCGTATCGCGAGTGC TACTCG CCTCTACTCA
	fB3	b-o*	GCACTCGCGATACGAGGCCTGG GCGTGAGGTGTCGATAGGTGCC
	fB4	o-c*-1*	GGCACCTATCGACACCTCACGC GAACGAATGGCTGCTGATCTGG AAACGG
S6-8	*B1x*	1x-c-a	CACCGTTT CCAGATCAGCAGCCATTCGTTC CAGTCCCAAGTCACCACCTAGC
	B2y	2y*-a*-b*-d2-3	GAGGATGT GCTAGGTGGTGACTTGGGACTG CCAGGCCTCGTATCGCGAGTGC TACTCG CCTCTACTCA
	fB3	b-o*	GCACTCGCGATACGAGGCCTGG GCGTGAGGTGTCGATAGGTGCC
	fB4x	o-c*-1x*	GGCACCTATCGACACCTCACGC GAACGAATGGCTGCTGATCTGG AAACGGTG
S5au	*A1x*	2*-a*-c*-1x*	GGATGT GCTAGGTGGTGACTTGGGACTG GAACGAATGGCTGCTGATCTGG AAACGGTG
	fA2au	c2-b-a-2y	GCCATTCGTTC GCACTCGCGATACGAGGCCTGG CAGTCCCAAGTCACCACCTAGC ACATCCTC
	fA3au	o-b*-T2-a	GGCACCTATCGACACCTCACGC CCAGGCCTCGTATCGCGAGTGC TT CAGTCCCAAGTCACCACCTAGC
	fA4au	c-o*-d2-3	CCAGATCAGCAGCCATTCGTTC GCGTGAGGTGTCGATAGGTGCC TACTCG CCTCTACTCA
S6au	*B1x*	1x-c-a	CACCGTTT CCAGATCAGCAGCCATTCGTTC CAGTCCCAAGTCACCACCTAGC
	fB2au	2y*-a*-b*-c2*	GAGGATGT GCTAGGTGGTGACTTGGGACTG CCAGGCCTCGTATCGCGAGTGC GAACGAATGGC
	fB3au	1x-c-b-o*	CACCGTTT CCAGATCAGCAGCCATTCGTTC GCACTCGCGATACGAGGCCTGG GCGTGAGGTGTCGATAGGTGCC
	fB4au	d1s-T2-o-c*-1*	CCAAACCTTCATCTTC TT GGCACCTATCGACACCTCACGC GAACGAATGGCTGCTGATCTGG AAACGG
R	*d*	TET-d	/5TET/ CTCCAAACCTTCATCTTCTACTCG
	q	3*-d*-IABkFQ	TGAGTAGAGG CGAGTAGAAGATGAAGGTTTGGAG /3IABkFQ/

Note: domain c = c1 + c2, d = 5'CT + d1s + d2, g = g1 + g2, j = j1 + j2, j2=5'G + j2s, 1x = 5'CA + 1, 2y = 2 + 3'TC.

References

(1) Zhang, D. Y.; Turberfield, A. J.; Yurke, B.; Winfree, E. *Science* **2007**, *318*, 1121-1125.

(2) Sabir, T.; Toulmin, A.; Ma, L.; Jones, A. C.; McGlynn, P.; Schröder, G. F.; Magennis, S. W. *J. Am. Chem. Soc.* **2012**, *134*, 6280-6285.

(3) Chen, X. *J. Am. Chem. Soc.* **2012**, *134*, 263-271.

(4) Reynaldo, L. P.; Vologodskii, A. V.; Neri, B. P.; Lyamichev, V. I. *J. Mol. Biol.* **2000**, *297*, 511-520.

(5) Srinivas, N.; Ouldridge, T. E.; Šulc, P.; Schaeffer, J. M.; Yurke, B.; Louis, A. A.; Doye, J. P. K.; Winfree, E. *Nucleic Acids Res.* **2013**, *41*, 10641-10658.

(6) Ladbury, J. E.; Sturtevant, J. M.; Leontis, N. B. *Biochemistry* **1994**, *33*, 6828-6833.

(7) Zhong, M.; Rashes, M. S.; Leontis, N. B.; Kallenbach, N. R. *Biochemistry* **1994**, *33*, 3660-3667.

(8) Zhang, D. Y.; Winfree, E. *J. Am. Chem. Soc.* **2009**, *131*, 17303-17314.

(9) McKinney, S. A.; Freeman, A. D. J.; Lilley, D. M. J.; Ha, T. *Proc. Natl Acad. Sci. USA* **2005**, *102*, 5715-5720.

(10) Dabby, N. L.: Synthetic molecular machines for active self-assembly: prototype algorithms, designs, and experimental study. PhD thesis, California Institute of Technology: California Institute of Technology, 2013.

(11) Lu, M.; Guo, Q.; Marky, L. A.; Seeman, N. C.; Kallenbach, N. R. *J. Mol. Biol.* **1992**, *223*, 781-789.

(12) Wang, J. S.; Zhang, D. Y. *Nat. Chem.* **2015**, *7*, 545-553.

(13) Zuker, M. *Nucleic Acids Res.* **2003**, *31*, 3406-3415.

(14) Kadrmas, J. L.; Ravin, A. J.; Leontis, N. B. *Nucleic Acids Res.* **1995**, *23*, 2212-2222.

(15) Wang, Y.; Mueller, J. E.; Kemper, B.; Seeman, N. C. *Biochemistry* **1991**, *30*, 5667-5674.

(16) Machinek, R. R. F.; Ouldridge, T. E.; Haley, N. E. C.; Bath, J.; Turberfield, A. J. *Nat. Commun.* **2014**, *5*, 5324.

(17) Olson, X.; Kotani, S.; Padilla, J. E.; Hallstrom, N.; Goltry, S.; Lee, J.; Yurke, B.; Hughes, W. L.; Graugnard, E. *ACS Synth. Biol.* **2017**, *6*, 84–93.

(18) Seelig, G.; Yurke, B.; Winfree, E. *J. Am. Chem. Soc.* **2006**, *128*, 12211-12220.

(19) Chen, X.; Briggs, N.; McLain, J. R.; Ellington, A. D. *Proc. Natl Acad. Sci. USA* **2013**, *110*, 5386-5391.

(20) Zadeh, J. N.; Steenberg, C. D.; Bois, J. S.; Wolfe, B. R.; Pierce, M. B.; Khan, A. R.; Dirks, R. M.; Pierce, N. A. *J. Compu. Chem.* **2011**, *32*, 170-173.

(21) You, Y.; Tataurov, A. V.; Owczarzy, R. *Biopolymers* **2011**, *95*, 472-486.

(22) Dirks, R. M.; Pierce, N. A. *Proc. Natl Acad. Sci. USA* **2004**, *101*, 15275-15278.

(23) Zhang, D. Y.; Winfree, E. *Nucleic Acids Res.* **2010**, *38*, 4182-4197.

(24) Cantor, C. R.; Warshaw, M. M.; Shapiro, H. *Biopolymers* **1970**, *9*, 1059-1077.

(25) Kick, A.; Boensch, M.; Mertig, M. *BMC Bioinformatics* **2012**, *13*, 138.